**The Effect of Anode Surface Structures on Microbial Fuel Cells**

Undergraduate Honors Thesis

Presented in Partial Fulfillment of the Requirements for Graduation with
Honors Research Distinction in the Department of Mechanical Engineering
at The Ohio State University

By

Clare Y. Cui

Advisor: Dr. Shaurya Prakash

**Abstract**

Wastewater treatment uses 3-4% of all electrical energy (approximately 820 million to 1.1 billion kWh) in the United States annually and is a promising source for energy and nutrient reclamation through microbial fuel cells (MFCs). MFCs are bio-electrochemical devices that use specific species of electrochemically-active bacteria as transporters of electrons for electrical power generation. The current maximum MFC power density of 3.32 $kWm^{-3}$ is low compared to its theoretical maximum of 53 $kWm^{-3}$, leaving much room for improvement. In this honors thesis, we hypothesized adding surface structures to the anode would tune shear rates at the anode surface independently of inlet flow rates, generating a more robust biofilm and, therefore, higher power output. The objective of this project was to design a continuous-flow MFC with structured anodes and determine the effect of anode surface structures on power output. A single chamber MFC was designed with three anode types: flat, patterned cylinders, and patterned cones. Designs were tested first in batch and then in continuous-flow at three flow rates: 0.12 $mLmin^{-1}$, 0.21 $mLmin^{-1}$, and 0.73 $mLmin^{-1}$. In batch, the cones and cylinders designs had thirteen and four times the peak power output of the flat design (0.27 $mWm^{-2}$) with 3.44 $mW·m^{-2}$ and 1.19 $mW·m^{-2}$, respectively. In continuous-flow, maximum attainable power density (MAPD) was highest for the cones design at all flow rates (3.75 $mWm^{-2}$, 3.23 $mWm^{-2}$, and 3.69 $mWm^{-2}$ from low to high flow rates) and was significantly larger than the MAPD of the cylinders (1.48 $mWm^{-2}$, 0.65 $mWm^{-2}$, 0.86 $mWm^{-2}$) and flat (1.09 $mWm^{-2}$, 1.31 $mWm^{-2}$, 1.15 $mWm^{-2}$) anode designs. From this research, it was determined that anode geometry does affect power output. The patterned cone design was selected as a potential design feature for future MFCs to increase overall power output while the patterned cylinders design was rejected. Overall, this work motivates further investigation into unique anode geometries as a design aspect for microbial fuel cells as a method of increasing power output.

# Table of Contents

# List of Tables

# List of Figures

## Chapter 1: Introduction

### 1.1 Need for Microbial Fuel Cells

When considering the long term future of our global society, developing infrastructure for sustainable energy is of pressing concern now more than ever before. Sustainable energy is energy that is derived from a source that, used in the present day, will not compromise access to energy in the future [1]. According to the International Energy Agency, the world demand for electricity will increase by more than 70% from 2015 to 2040 [2][2], and Figure 1 shows this clear trend starting from 1980 projected to 2040. Currently, 86% of global energy is generated through fossil fuels [3]. Oil and gas, which contribute to 63% of total energy generated, are expected to be depleted by 2068 based on total estimated reserves in 2015 [3]. Due to this fossil fuel consumption, 29 Gt of carbon dioxide are produced each year, where 10.2 Gt are released into the atmosphere, contributing to greenhouse gas effects, and, subsequently, global warming and climate change [[3], [4]]. Since fossil fuels are a finite resource and their consumption for energy have a largely detrimental effect on the environment, investigating sustainable, carbon-neutral sources of energy for the future and methods of implementing them is of great importance.
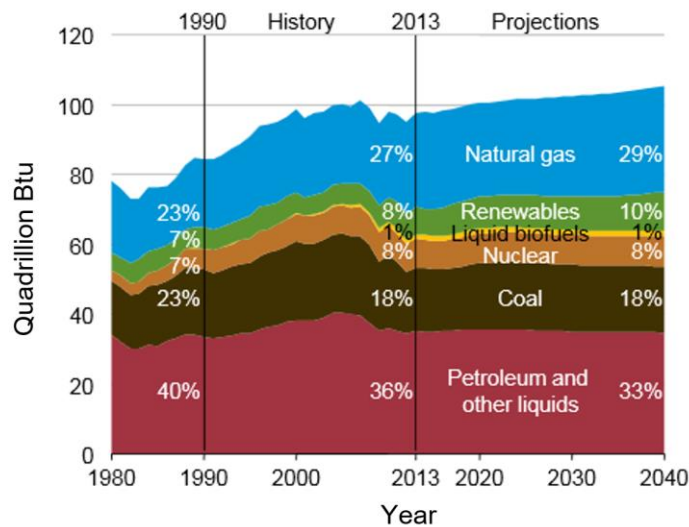


***Figure 1:*** *Primary energy consumption by fuel in the United States from 1980 projected to 2040 in quadrillion Btu* [6].

Alongside our concerns for our dependence on fossil fuels, water and its sustainability is also a point of focus for the health of our society, both now and later. Freshwater is a valuable resource, where approximately 306 billion gallons were used each day in the United States in 2010, with 90% being surface water withdrawals [7]. However, when surface water is not available, groundwater must be used [8]. In 2011, California entered a four year drought where surface water became much scarcer, resulting in a water supply composed of 60% groundwater as opposed to the more typical 30-40% [8],[9]. These situations can lead to negative long-term effects such as land subsidence, aquifer infrastructure damage, and seawater intrusion which could compromise groundwater quality [9]. Furthermore, shrinking freshwater sources such as the Ogallala Aquifer, which reaches from South Dakota to Texas, are putting approximately one-fifth of the United States' cattle, corn, cotton, and wheat at risk [[10], [12]]. As of 2012, approximately 40% of the aquifer was reported to be depleted with a continuing state of steady decline from intensive agricultural use and slow recharge rates, essentially meaning that the water in the aquifer is a non-renewable resource [[12], [10]]. In order to fulfill the increasing need for freshwater resources, it is imperative that infrastructure is investigated and developed to keep freshwater readily available and from further burdening the natural landscape.

Wastewater treatment may be a potential direct source for obtaining freshwater. It is estimated that 99.9% of all wastewater is water and is recyclable [11]. Typically, water is drawn from lakes, rivers, aquifers, and groundwater for use, with a majority of wastewater returned back to the environment after being treated [12],[14]. Public and municipal users return 75-85% and industrial users return 80-90% of withdrawn water [14], [16]. Water reuse systems, which treat and convert wastewater to freshwater on-site, have been shown to be as safe and potable as water brought through the conventional environmental buffer, such as lakes and rivers [[13], [11],[14]].

2

The high return and success of advanced wastewater treatment proves there is a ready source that would benefit from immediate treatment at the point of use, and doing so would reduce energy and monetary costs in pumping and storage. Despite this, water reuse systems are still more expensive than drawing from freshwater sources, with costs varying depending on a variety of conditions, such as location, treatment methods used, water quality standards, and more factors [13]. Therefore, there is still much room to make these processes more energy efficient so that water reuse and advanced treatment of wastewater become a mainstream method of treating water.

The demands for energy in wastewater treatment in the present day are considerable. The most used process in wastewater treatment is activated sludge treatment [11] which purifies wastewater by exposing organic waste matter and microorganisms to oxygen *via* aeration, causing microbes to breakdown organic matter, releasing carbon dioxide, water, and energy in the process [15]. Unfortunately, this process has a high energy cost of 0.5 $kWh^{-1}m^{-3}$ due to the aerobic processes involved [11][12]. Currently, electrical energy used for wastewater treatment comprises 3-4% of the energy consumed in the United States each year, which equated to approximately 8.2 $\times 10^8$ to $1.1 \times 10^9$ kWh in the year 2015 [[16], [17]]. While it takes energy to treat water, it is also feasible to reclaim energy from the treatment process. Domestic wastewater has the potential to yield up to 2.2 $kWh^{-1}m^{-3}$ in aeration [11]. To take advantage of this energy potential, microbial fuel cells can be used, which have been shown to be able to use wastewater to generate electricity [[11], [12]].

## 1.2 The Microbial Fuel Cell and Application in Wastewater Treatment

Microbial fuel cells are bio-electrochemical devices that use microorganisms to convert chemical energy in organic compounds into electricity [18]. In the anode chamber of a microbial fuel cell, bacteria oxidize substrates, producing electrons, protons, and $CO_2$ [18]. Substrates are

either replenished intermittently, referring to batch-fed mode, or constantly in a fluid flowing into and out of the anode chamber, which refers to continuous-flow mode.

Bacteria exist in the anode chamber either suspended in the fluid or in a biofilm on the anode itself [19]. For the majority of the existence of microbial fuel cells, mediators such as thionine, methyl viologen, and others were used to shuttle electrons between the bacteria and electrode [20]. However, in 1999, it was discovered that *Shewanella putrefaciens* was capable of directly transferring electrons due to electron carriers on the cell surface, resulting in the mediator-less MFC [21], with the bacteria themselves being known as exoelectrogens or electrochemically-active bacteria [21]. Electrons, therefore, can be transferred to the anode through a variety of methods, including electron mediators, direct bacteria membrane transfer, or by conductive nanowires produced by bacteria [[22], [23], [24]]. Direct interspecies electron transfer has also been shown to be another way for current production, although it is not well understood yet [32]. However, it is preferable to use mediator-less MFCs since synthetic mediators are toxic and unstable, which would be unsuitable in an application setting such as wastewater treatment [18].

Once transferred, electrons travel through an external circuit to the cathode. Protons in the anode chamber cross a proton exchange membrane (PEM), where they combine with oxygen and electrons in a reduction half-reaction to form water. Bacteria in the anode must be kept in an anaerobic environment in order to prevent electrons from reaching any other end acceptor besides the anode itself [18]. Figure 2 shows the operations of an air-cathode MFC with chemical half-cell reactions at the anode and cathode.
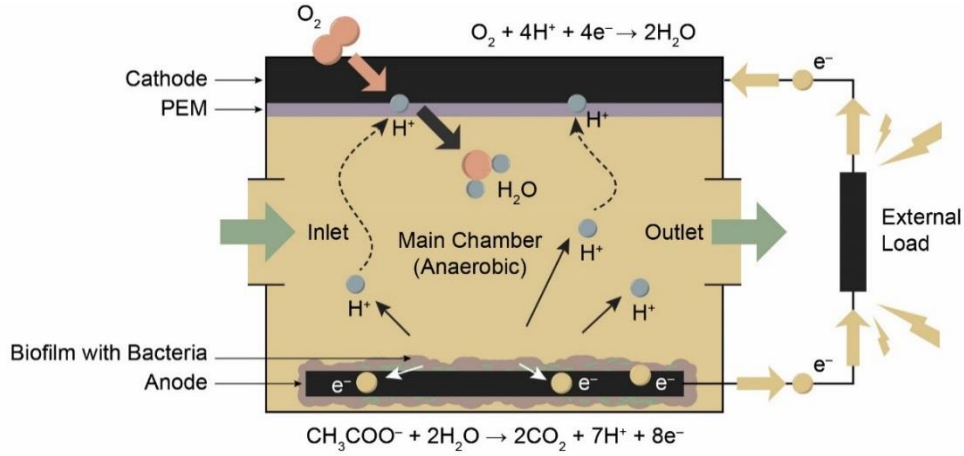
*Figure 2: Schematic for an air-cathode MFC in operation showing the oxidation reduction reactions and transfer of electrons leading to generation of an electric potential that can be harvested at an external load* [25].

These chemical reactions compose the two halves of a reduction-oxidation reaction and allow for the generation of an electric current. At the anode, a reduction half-cell reaction occurs, and, at the cathode, an oxidation half-cell reaction occurs [25]. These reactions are given below using acetate. Acetate is a common electron donor used with anaerobic bacteria and is a predominant fuel source for MFCs [[26], [27]]. Thus, the chemical equation (Equation 1) for the oxidation half-reaction at the anode using acetate [18] is given as:

$$CH_3COO^- + 2H_2O \rightarrow 2CO_2^- + 7H^+ + 8e^- \tag{1}$$
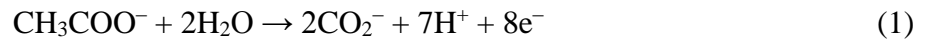
At the cathode, the reduction half-reaction equation (Equation 2) [18] is given as:

$$O_2 + 4H^+ + 4e^- \rightarrow 2\ H_2O \tag{2}$$

Microbial fuel cells have clear benefits for the current wastewater treatment system in place of the energy-intensive activated sludge treatment. Their implementation could simultaneously degrade waste and reclaim energy for further use at the plant. It has been shown that, using wastewater as the anode effluent, MFCs can degrade 50-90% of the organic waste [[28], [29], [30]]. Additionally, MFCs have the added advantage of being carbon-neutral, with the $CO_2$ that is released in the oxidation reaction originating from biomass that used photosynthesis to obtain it from the

atmosphere [18]. Since electrochemically-active bacteria is already abundant in wastewater treatment centers [31], it is clear that MFCs would be a worthy installment in this application by simultaneously increasing energy efficiency and keeping the functionality of the original system intact.

## 1.3 Causes of Low Power Output

Despite the widespread benefits of implementation of microbial fuel cells in a wastewater treatment plant, application of MFCs have been stalled by low power output. The theoretical maximum for MFCs with a surface area to volume ratio (*SA/V*) of $10^3$ m$^{-1}$ that is limited by the cathode surface area is approximately 53 kWm$^{-3}$ [32]. The current maximum power density achieved thus far is 3.32 kWm$^{-3}$, with an actual power output of $4.15 \times 10^{-5}$ W, where the MFC was miniaturized with a working anode volume of 0.0125 cm$^3$ [33]. With more than one order of magnitude of power density in difference, MFC technology still has much more room for improvement.

Microbial fuel cells lose voltage for a variety of reasons. Air-cathode MFCs using acetate have a maximum MFC voltage, or electromotive force (EMF) voltage, of 1.1 V, which is the difference between the electrode potential, where $E_{cell} = E_{cat} - E_{an}$ [[32], [25]]. However, due to overpotentials at the anode and cathode as well as ohmic losses, the emf voltage can never be obtained. The actual cell voltage is the emf voltage subtracted by overpotentials and the ohmic losses [34]. Activation losses and mass transport losses, which are contributors to electrode overpotential, as well as ohmic losses are the most relevant to this thesis [34].

Ohmic losses are due to resistance to the electrons through the electrodes and internal connections as well as resistance of the protons through the anolyte solution and PEM [32]. These losses are some of the most important ones to overcome in order to create the optimal MFC design.

6

Improvements can be made by decreasing electrode spacing, using a PEM with low resistivity, ensuring good contact, and increasing solution conductivity [34]**Error! Reference source not found.**. Activation losses arise when there is a transfer of electrons at the anode surface, either due to a compound reacting at the bacterial surface, at a mediator, or at the final electron acceptor at the cathode and are apparent at low current densities, as can be seen in Figure 3 [32]. These losses can be mitigated by increasing electrode surface area, increasing the internal temperature of the MFC, creating an enriched biofilm on the anode, and by improving electrode catalysis [34]. Mass transport losses occur at high current densities (refer to Figure 3), where there is a limited mass transfer of reactants to the electrode and, therefore, low substrate flux, resulting in a limited rate of reaction [32]. This type of loss can sufficiently be avoided by operating the MFC in continuous-flow mode [32]. In order to create a successful MFC device, these overpotential and ohmic losses should be taken into consideration at both the design and operation stages in order to reduce power loss and obtain the best efficiency possible.
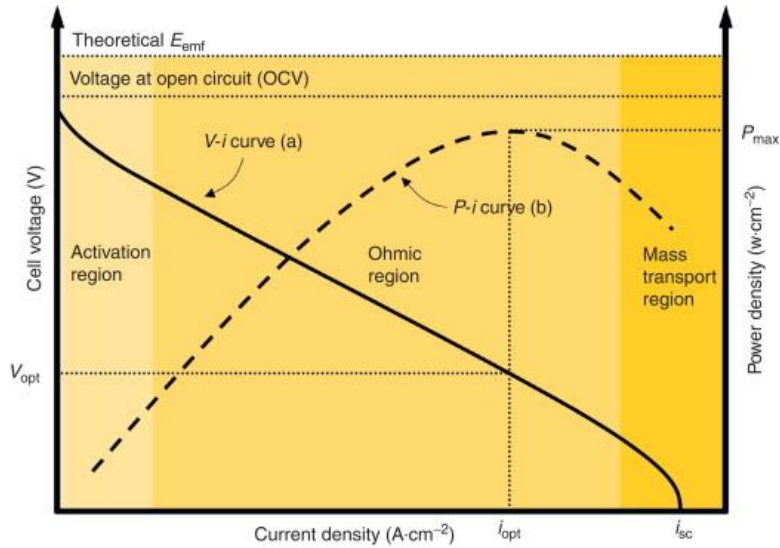


***Figure 3:*** *Example (a) polarization and (b) power curves for MFCs, Maximal Attainable Power Density (MAPD) is show by $P_{max}$, which corresponds with optimal voltage ($V_{opt}$) and optimal current ($i_{opt}$). Short circuit current $i_{sc}$ is reached at zero external resistance [11].*

**1.4 Possible Factors Affecting Biofilm Development**

A biofilm is a community of microbes that attaches irreversibly to surfaces and is enclosed in a primarily polysaccharide material that forms a polymeric matrix [35]. It is essential to have a stable, enriched biofilm for increased power output between the bacteria and anode, and this state is reached when a sustained current generation is established [36]. The biofilm is a 'micro'-ecosystem where a mixed culture of microbial species work together to protect themselves against stresses in the environment and more efficiently distribute nutrients [37]**Error! Reference source not found.**. The stability of a biofilm is directly linked to the adhesion strength of the bacteria, where surface proteins such as pili and flagella make contact with the electrode and adhere through oxidation, hydration, and other chemical reactions [38], [39]. Surface properties of anodes also have an impact on adhesion, where, for example, it was shown that graphite foam electrodes having the same geometric surface area as graphite rods had a higher concentration of cells by a factor of 2.7 [40].

The hydrodynamic shear rate of a fluid flowing over the biofilm also plays a role in bacterial adhesion [38]. When under continuous-flow conditions, there is a possibility for localized biofilm detachment if high shear stresses exceed the tensile adhesion strength of the biofilm [**Error! Reference source not found.**[38], [41]]. However, it has also been shown that a larger hydrodynamic shear rate results in shear stress to the biofilm, causing it to grow denser and to generate greater power output. In one study done by Pham, a low shear rate of 80 s$^{-1}$ resulted in a power density of 50 Wm$^{-3}$ while a high shear rate of 120 s$^{-1}$ had a power density of 160 Wm$^{-3}$ [41]. In terms of scaling factors, the high shear rate, which was 1.5 times the low shear rate, resulted in a power density that was 3.2 times the low shear rate power density [41]. In addition to this power difference, confocal laser scanning microscopy and scanning electron microscopy were used to

determine biofilm density, which doubled from 0.73 $\mu m^3$ of biomass per $\mu m^2$ of anode surface to 1.52 $\mu m^3$ of biomass per $\mu m^2$ of anode surface, showing that an increase in shear rate could create a denser biofilm that had a greater adhesion to the MFC anode [41].

One approach that could potentially further enrich the biofilm is to look at nature for inspiration. In sea coral and bovine rumen, high bacterial concentrations can be found. For sea coral, this ranges from $10^5$ to $10^6$ cells·mL$^{-1}$ [42]**Error! Reference source not found.** and, for bovine rumen, this ranges from $10^9$ to $10^{10}$ cells·mL$^{-1}$ [43]. One commonality shared between these biological entities is that both have unique structures that enable the capture and retaining of bacteria. Both are composed of complex geometries that project outwards into their environment (Figure 4a and 4b). Since MFCs are also exposed to similar hydrodynamic shearing forces like corals and algae, it was natural to take inspiration from these structures and implement them into MFCs.



(a)                                                        (b)

*Figure 4: (a) Halocynthia roretzi sea coral [44] and (b) bovine rumen [45] lining have high bacterial concentrations that serve as bio-inspiration for MFC anode surface design.*

### 1.5 Previous Work from Our Group

Previous work and collaboration with Matthew Gerber (MS, 2014 Mechanical Engineering, Ohio State) resulted in three anode surface structure designs as well as a complete set of MFC testing results against which this study could be compared. There were two aspects of

the previous project, with one being a numerical analysis conducted on various structure geometries and an experimental analysis of actual surface structures being implemented in the anode of the MFC. The numerical and experimental results conflicted with each other unexpectedly, which was partially responsible for motivating this thesis work.

In the numerical analysis, 40 structural designs were initially analyzed in COMSOL Multiphysics v.4.3b in order to determine the effects of geometry on surface shear rates. Each design was tested with one structure set inside a simple rectangular channel with three different Reynolds numbers of $10^{-3}$, 0.1, and 10. A dimensionless surface shear rate magnitude that was averaged over selected surfaces was used as the quantitative metric for the comparisons. From this, the five structures with the highest shear rate magnitudes were chosen to be modeled in $4 \times 4$ arrays. Based on this, the cylinder and cone designs were chosen for their more simplistic designs due to their machinability as well as the ability to distinguish between their average shear rate magnitudes. The flat design was also chosen to use as a baseline comparison against the other designs. Finally, all three of the selected anode designs were modeled with the MFC anode chamber geometry as $4 \times 4$ arrays (Figure 5). It was found that the flat anode base surface had a higher shear rate magnitude than either of the bases of the patterned cylinder and patterned cone designs since it was not obstructed by structures. The top facets of the cylinders exhibited the greatest values of shear rate magnitude although those values were also higher for the cone at its top facets. In general, it was expected that the biofilm would be the densest and thinnest on the surface structures themselves as opposed to their base and that there would be no locational preference for bacteria colonizing on the flat anode.

10
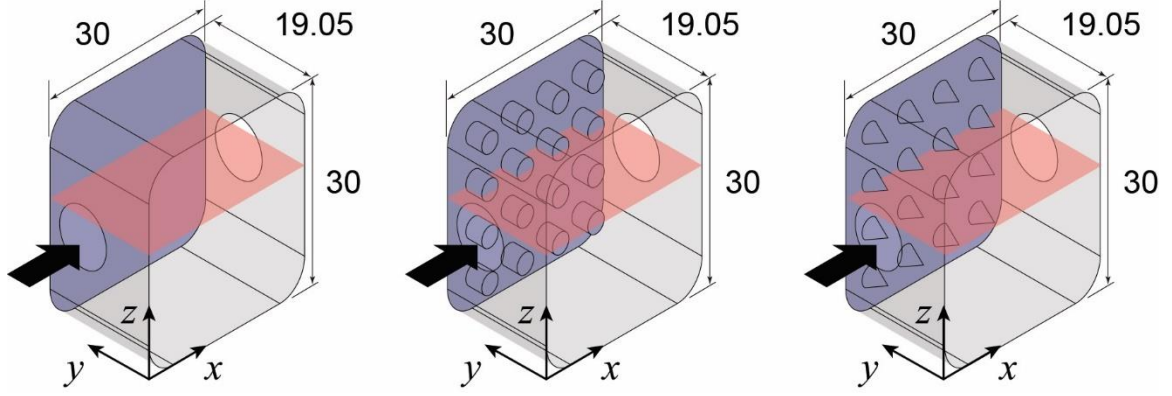
*Figure 5: Numerical analysis and flow simulation for three anode designs situated in the designed MFC. From left to right, flat, patterned cylinders, and patterned cones* [25].

Upon finishing the numerical analysis, the MFC was designed and constructed with the selected surface structures in mind. Per design, measurements in batch-fed mode were measured for one day prior to 50 hours of continuous-flow mode, with a resistance sweep (see Section 3.4) conducted at the end of continuous-flow testing. External resistances used ranged from 80–8000 $\Omega$. In batch-fed, where there was no surface shearing, the results were exactly as expected, based on electrode spacing and wetted surface area, in which a smaller electrode spacing and larger surface area would have both increased power output. The flat anode had the lowest power output at $9.1 \times 10^{-5}$ mW, followed by the cone with $3.0 \times 10^{-4}$ mW, and the cylinder had the largest power output at $1.3 \times 10^{-3}$ mW. In continuous-flow mode, however, these results did not match with the theory as well. The flat anode was seen to obtain the highest average power output at $7.46 \times 10^{-3}$ mW, followed by the cylinder design at $2.68 \times 10^{-3}$ mW, with the lowest average power output at $7.12 \times 10^{-4}$ mW by the cone design. These trends did not follow the same theory that worked for the batch-fed feeding mode, in which electrode spacing and surface area were not determining factors for power output. Additionally, the shear rate magnitude did not appear to scale, where the shear rate magnitude of the flat anode was just 1.08 times that of the cone design, but the power output was 10.58 times that of the cone.

*Table 1: Summarized results from previous work by Matthew Gerber. Contains all pertinent information characterizing the MFC system based on anode design, shear rate magnitude, batch-fed and continuous-flow results* [25].

| | Metric | Flat | Cylinder | Cone |
|---|---|---|---|---|
| **System** | Anode Wetted Surface Area [cm$^2$] | 8.81 | 13.9 | 10.4 |
| | HRT [h] | 2.00 | 1.95 | 1.98 |
| | Chamber Volume [mL] | 16.8 | 16.4 | 16.6 |
| | Electrode Spacing [mm] | 19.05 | 18.75 | 18.75 |
| $\gamma_s$ | Entire Wetted Surface of Anode | $1.73 \times 10^{-6}$ | $1.62 \times 10^{-6}$ | $1.60 \times 10^{-6}$ |
| | Only Flat Anode Base | $1.73 \times 10^{-6}$ | $0.78 \times 10^{-6}$ | $1.11 \times 10^{-6}$ |
| | Only Structural Elements | n/a | $2.72 \times 10^{-6}$ | $2.91 \times 10^{-6}$ |
| **Batch-fed** | Peak Output Power [mW] | $9.1 \times 10^{-5}$ | $1.3 \times 10^{-3}$ | $3.0 \times 10^{-4}$ |
| | Peak Power Density [mW/m$^2$] | 0.10 | 0.93 | 0.29 |
| | Peak Power Density [mW/m$^3$] | 5.43 | 78.6 | 18.0 |
| **Continuous-flow** | Average Power Output [mW] | $7.46 \times 10^{-3} \pm$ $(2.07 \times 10^{-4})$ | $2.68 \times 10^{-3} \pm$ $(1.7 \times 10^{-5})$ | $7.12 \times 10^{-4} \pm$ $(1.7 \times 10^{-5})$ |
| | Average Power Density [mW/m$^2$] | $8.63 \pm$ $(1.7 \times 10^{-3})$ | $1.97 \pm$ $(2.1 \times 10^{-4})$ | $0.70 \pm$ $(7.8 \times 10^{-4})$ |
| | Average Power Density [mW/m$^3$] | $452.7 \pm$ $(8.9 \times 10^{-2})$ | $166.7 \pm$ $(1.8 \times 10^{-2})$ | $43.7 \pm$ $(4.9 \times 10^{-2})$ |
| | MAPD [mW/m$^2$] | 9.05 | 2.69 | 1.45 |
| | $R_{ex}$ at MAPD [k$\Omega$] | 0.98 | 1.76 | 3.85 |
| | Internal Resistance, $R_{int}$ [k$\Omega$] | 1.02 | 1.96 | 4.10 |
| | OCV [mV] | 187.5 | 173.5 | 156.0 |

Abbreviations: HRT = Hydraulic retention time, $\gamma_s$ = Dimensionless shear rate magnitude averaged of a surface of interest, OCV = Open-circuit voltage, MAPD = maximum attainable power density

These results can be explained through some of the theoretical observations as well as in other aspects of the experiment. A primary factor might have been that, despite the continuous-flow regime, there were still areas that were diffusion-limited. Due to the surface structures, there were recirculation regions where the substrate was never able to be replenished, which is represented with black spiraling lines and enclosed contours in the areas near the inlet and outlet in Figure 6. With no fresh substrate, bacteria would be less likely to form a survivable biofilm in

these zones, therefore decreasing power output for the anode designs with surface structures. Based on these inconclusive continuous-flow results, it was necessary to re-test this previous work for verification that the results obtained were true or as previously expected.
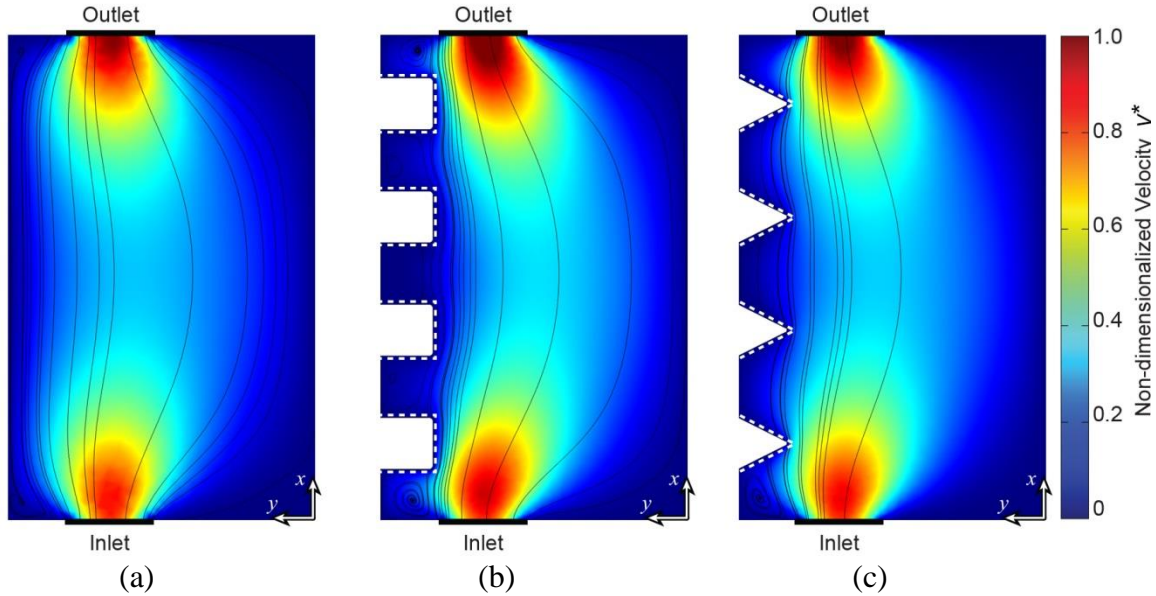


*Figure 6: Velocity plots of (a) flat, (b) cylinder, and (c) cone designs in a 2D cross section showing the side profile of the MFCs. Streamlines are indicated with black lines for the x and y components of velocity, which is non-dimensionalized* [25].

## 1.6 Thesis Statement

Based on the interaction between the biofilm that grows on the anode in an MFC and hydrodynamic shearing forces that occur within a continuous-flow environment, there is reasonable cause to investigate how to enable the biofilm to handle higher shearing stresses inherently through MFC design. From nature, there are successful examples of biological structures such as sea coral and bovine rumen lining that have high concentrations of bacteria that are constantly subjected to fluid flow. In this thesis, we are interested in investigating the manipulation of anode surface geometry to mimic nature in order to produce improved power output.

The objective of this project is twofold. The first goal is to design a microbial fuel cell capable of operation in batch-fed and continuous-flow feeding modes that is modular and allows different anodes to be used with varying surface geometrical designs. The second goal is to determine the effect of geometrical alterations to the anode on the power output of the designed microbial fuel cell at varying flow rates.

## Chapter 2: Design of the Microbial Fuel Cell

There were several design and material decisions to be made when designing the MFC for this project. The H-design, two-chamber, and single chamber designs are the most common types of MFCs and can be seen in Figure 7. H-design MFCs (Figure 7A) are inexpensive, quick-build designs that consist of two bottles connected with a salt bridge or other PEM [34]. They are commonly used in a laboratory setting for basic parameter research, and have low power densities due to high internal resistance [34]. Since H-design fuel cells are fed in batch, they were unsuitable for this project, which required feeding by continuous-flow.

The two-chamber MFC and single-chamber MFC (Figure 7B and Figure **7**C) designs differ primarily in that the two-chamber MFC has a separate cathode chamber containing a catholyte solution that has an electron acceptor, which is typically dissolved oxygen or ferricyanide [46]. The two-chamber MFC design is also very closely related to an H-design, where most are fed in batch, although there have been MFCs developed that allow for continuous-flow and the two-chamber MFCs typically have higher power output as a result [47]. However, there are some drawbacks to the two-chamber design. Although using a ferricyanide catholyte solution can increase cell voltage, it is not sustainable as ferricyanide must be externally regenerated when exhausted [46]. Oxygen also must be continuously replaced in the cathode chamber by bubbling, thereby using more energy [46].
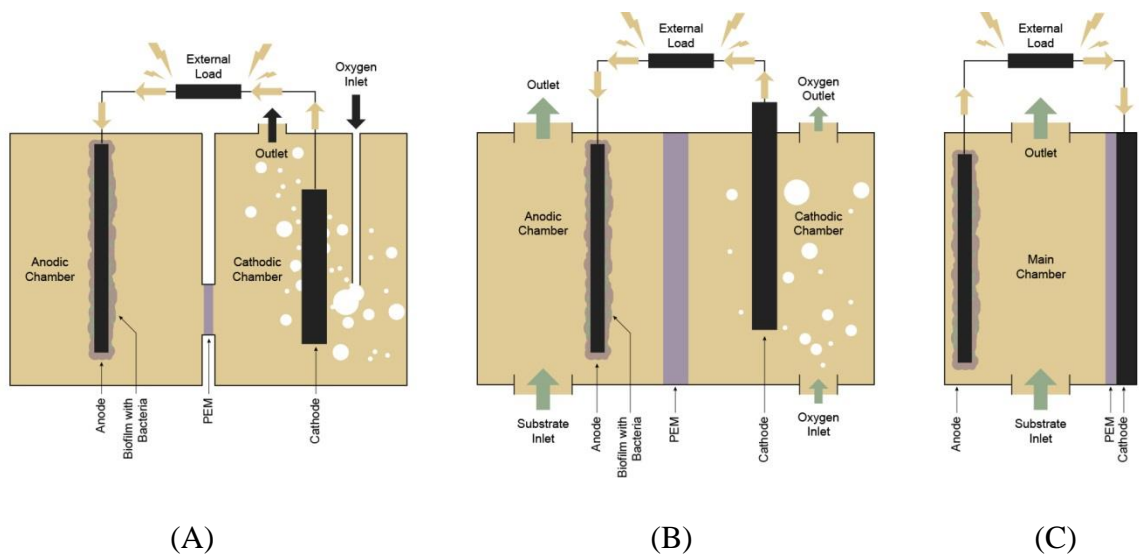
***Figure 7:*** *Different design schematics for MFCs. (A) H-design, (B) Two-chamber block design, and (C) single-chamber block designs are shown* [25].

Single-chamber or air-cathode MFCs have been shown to have even larger power densities than two-chamber MFCs due to lower internal resistance [34], [46]. These MFC types can be operated in both batch-fed and continuous-flow modes and are exposed to atmospheric oxygen, which also contributes to a higher power output since there are no issues with mass transfer rates of oxygen to the cathode [25]. Drawbacks to this design include difficulties in scale-up, where expanding the distance between electrodes would make power generation impossible and stacking these MFCs would require constant cathode exposure to air, possibly creating complicated, bulky MFC systems [25].

For the purpose of this experiment, a single-chamber MFC design was selected. In order to properly observe the effects that shear rate as on anode surface structures and resultant power output, it was necessary to have a continuous-flow environment. Implementing a single-chamber design also decreased costs and created a more simplistic design, as it was not necessary to develop a catholyte solution and use more time and resources to create a cathode chamber.

The design of the MFC was a block design originally designed in Solidworks 2012 (Figure 8), and all of the machined parts besides the patterned cylinders and patterned cones anodes were created by machinists at the Mechanical & Aerospace Engineering Machine Shop in Scott Laboratory according to design specifications which can be found in Appendix C. The patterned anodes were fabricated with a CNC mill in the Machine Shop of the Physics Department at The Ohio State University.
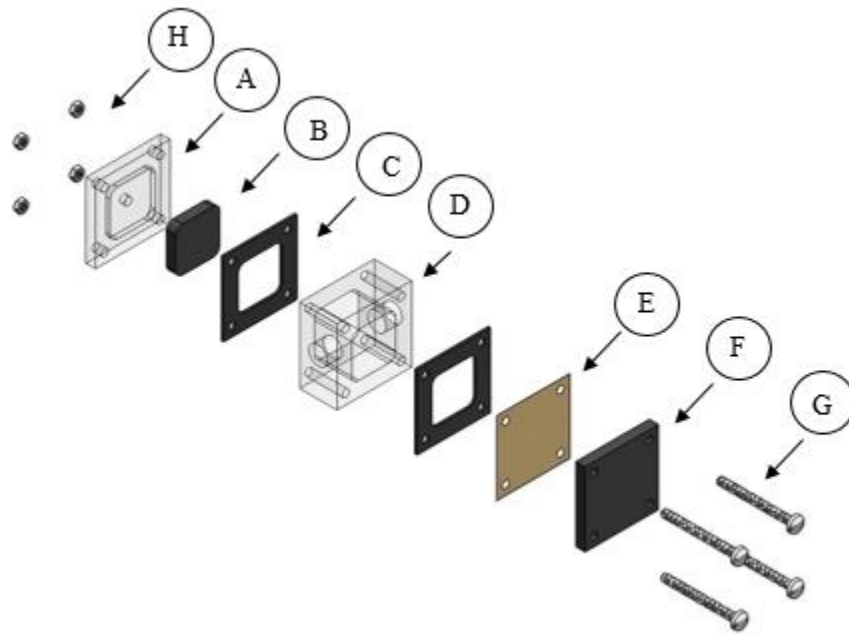


**Figure 8**: Microbial fuel cell design, created in Solidworks 2012. Design consists of (A) acrylic anode end plate, (B) graphite anode, (C) Two (2) butyl rubber gaskets, (D) acrylic anode chamber, (E) Ultrex CMI-7000 proton exchange membrane, (F) graphite cathode, (G) four (4) nylon 10-32 screws and corresponding (H) four (4) hex nuts.

The anodes were made from stock graphite plate, which was chosen for its defined surface area, machinability, good electrical conductivity, and relatively low material costs [48]. The cathode was also machined from the same graphite plate with no catalyst applied and had a thickness of 0.64 cm and a cross-sectional area of 24.29 $cm^2$. It is worth noting that, because of the thickness of the cathode plate, oxygen had low mass diffusivity through the graphite, estimated

to be between the orders of $10^{-9}$ to $10^{-16}$ cm$^2$/s [[48], [49]]. This caused the MFC to have an increased internal resistance that decreased overall power output. However, since the objective of this thesis was to determine how structural anode geometries affected power output amongst their own designs and not to increase MFC power to its optimal output, we did not seek improvements to this limitation and continued with the original design. The anode end plate and anode chamber were made from optically-clear cast acrylic, and the proton exchange membrane used was the Ultrex CMI-7000 (Membranes International, Ringwood, NJ). The MFC assembly was kept sealed and leak-proof with two butyl rubber gaskets placed in between the anode end plate and the anode chamber and the anode chamber and PEM. Nylon 10-32 screws and hex nuts held the entire assembly together; nylon was chosen so that no short circuits occurred between the anode and the cathode.
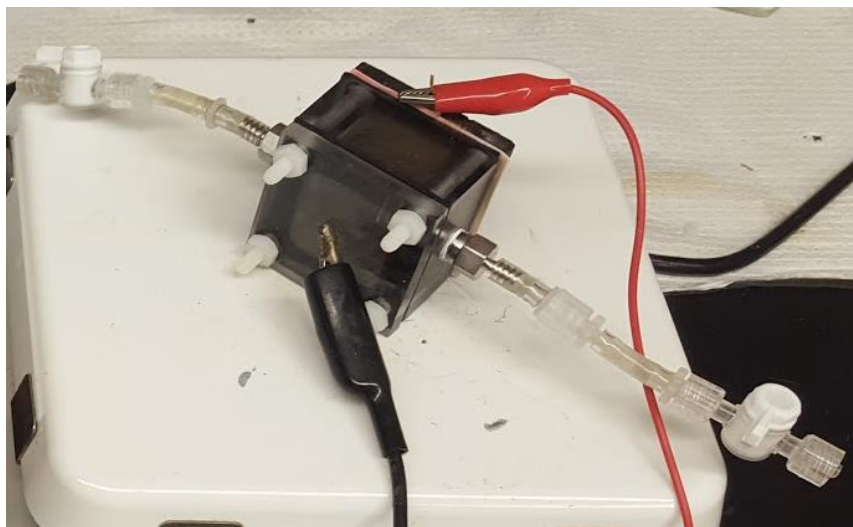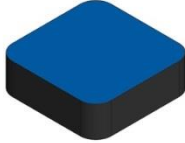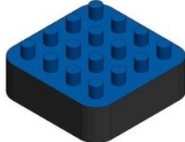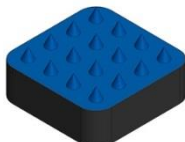


*Figure 9: Assembled MFC with connections to external resistance and digital multimeter (not shown).*

Once machined, the following procedure was conducted to clean the anodes [51]. They were first bathed in 5% nitric acid and boiled for one hour at a hot plate temperature of 300°C. Afterwards, they were soaked in DI water for 15 minutes and dried on a hot plate at 110°C for approximately 8 hours. CW2400 silver-based conductive epoxy (Chemtronics®, Kennesaw, GA)

18

was used to connect a platinum wire to the anode to create an electrical connection for the alligator clips to the external resistor and DMM. The epoxy was cured by setting the anode on a hot plate at 150°C for 10 minutes and then curing it at room temperature for approximately 18 hours afterwards. The anodes were then adhered to the acrylic anode end plates using Double/Bubble® Orange epoxy (Royal Adhesives and Sealants, South Bend, IN), where they were set into the end plate pockets to prevent leakage. The anode assemblies were heated on a hot plate at 150°C for 10 minutes and cured at 25°C overnight. Table 2 shows relevant information concerning the three anode designs and their physical volumes and surface areas.

**Table 2:** *Shown are anode designs for MFC. The cylinders design had the highest volume and surface area, followed by the cones design, and, lastly, the flat anode design. The wetted surface area is the area that comes into contact with the bacteria and substrate feed inside the anode chamber* [25].

| Design | Image | Anode Volume [cm$^3$] | Total Surface Area [cm$^2$] | Wetted Surface Area [cm$^2$] |
|--------|-------|------------------------|------------------------------|-------------------------------|
| Flat | | 8.66 | 29.0 | 8.81 |
| Cylinders | | 9.07 | 34.1 | 13.9 |
| Cones | | 8.80 | 30.6 | 10.4 |

## Chapter 3: Methodology

### 3.1 Bacteria, Nutrient Feed, and Reducing Agent

Bacteria were obtained from the rumen of a fistulated Jersey cow at the Waterman Dairy Farm, a research farm at The Ohio State University. To prepare the bacteria, rumen fluid and partially digested feed was squeezed through two layers of cheese cloth prior to being transported in cap-screw containers maintained in warm water at 40 ℃, which is the body temperature of a cow. The centrifuge was spun at 5000 g for 10 minutes to separate the pellet from the supernatant, with the supernatant used as the microbial inoculum for the MFC. Unused rumen fluid was stored at -78 ℃ with 8% DMSO to preserve the bacteria in the Ruminant Nutrition Laboratory under Dr. Jeffrey Firkins at Ohio State University. This bacteria was chosen since it had been previously shown to be electro-chemically active [19]. Inoculation into the MFC occurred at 1% v/v with respect to the substrate feed. This concentration was selected based off of concentrations of ingredients in the nutrient feed formula, both of which were derived from the Wang study in 2014 [52].



*Figure 10: Retrieving rumen fluid from a fistulated cow at the Ohio State University Research Farm.*

The nutrient feed used consisted of a simple salt solution, deionized water, and sodium acetate. Deionized water served as a solvent, and the acetate in the sodium acetate was the electron donor or substrate to be oxidized by the bacteria. The salt solution consisted of monopotassium

phosphate, ammonium chloride, sodium chloride, and magnesium sulfate, which were all used to support bacterial growth and provide essential nutrients. This formula was derived from Dr. Ann Christy's laboratory and can be seen in Table 3 [19].

**Table 3:** *1L formula of nutrient feed with DI water as a solvent, various salts for bacterial growth, and sodium acetate as the substrate* [25].

| Component | Formula | Amount | Concentration | Function/Role |
|---|---|---|---|---|
| DI water | $H_2O$ | 1000 mL | — | Solvent |
| Sodium acetate | $C_2H_3NaO_2$ | 5 g | 61.0 mM | Electron donor |
| Monopotassium phosphate | $KH_2PO4$ | 0.9 g | 6.61 mM | Salt for growth |
| Ammonium chloride | $NH_4Cl$ | 0.73 g | 13.6 mM | Salt for growth |
| Sodium chloride | NaCl | 0.9 g | 15.4 mM | Salt for growth |
| Magnesium sulfate | $MgSO_4$ | 0.09 g | 0.75 mM | Salt for growth |

A reducing agent was necessary in order to eliminate any excess oxygen inside the MFC. The reducing agent formula consisted of 0.4 M sodium hydroxide as the solvent, cysteine-hydrochloride as an oxygen scavenger, and aqueous sodium sulfide as another oxygen scavenger. The full formula can be seen in Table 4. When creating the continuous-flow feed formula, reducing agent was always added as 5% v/v of the nutrient feed. Therefore, for every 1L of nutrient feed created, 50 mL of reducing agent was added.

**Table 4:** *50 mL formula for reducing agent, which includes sodium hydroxide as a solvent and cysteine-hydrochloride and sodium sulfide as oxygen scavengers* [25].

| Component | Formula | Amount | Function/Role |
|---|---|---|---|
| 0.4 M Sodium hydroxide | NaOH | 30 mL | Solvent |
| Cysteine-Hydrochloride | Cys-HCl | 1.35 g | Oxygen scavenger |
| Aqueous 3% sodium sulfide | $Na_2S$ | 20 mL | Oxygen scavenger |

## 3.2 Batch-fed Methodology

Initially, the MFC was fed in batch a minimum of three days to allow colonization of the anode and anode chamber. The MFC was situated on top of a hot plate set at 55 ºC in order to

maintain an internal temperature of 40 ℃ [25] and was covered in insulation. Platinum and gold

wires on the anode and cathode, respectively, were connected to a decade box with a resistance

at 1000 Ω. A Keithley Digital Multimeter (DMM) measured the voltage in parallel with the

external resistance. This testing set up can be found in                                                    *(a)*

*(b)*

**Figure 11**.



(a)                                                                                      (b)
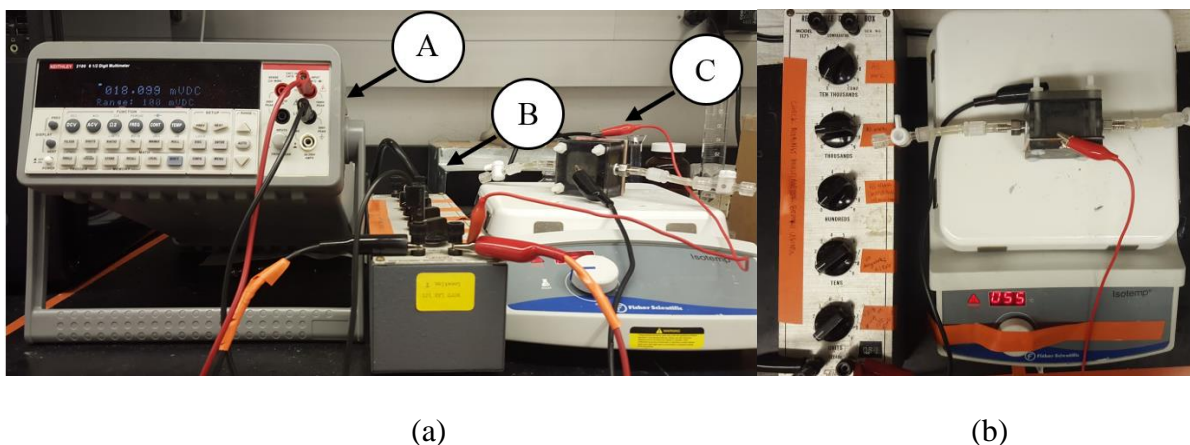
*Figure 11: MFC operating in batch-fed mode. (a) shows a front-view of the experimental set up and (b) shows a top view of the MFC and decade box. The (A) DMM was connected in parallel with the (B) external resistance set to 1 kΩ which connected the anode and cathode of the (C) MFC using alligator clips. The MFC was set on a hot plate set to a temperature of 55 °C*

The MFC was fed approximately once every 24 hours. Each time the MFC was fed, 20%

of the chamber volume was replaced with substrate feed, along with an additional 5% v/v of

reducing agent to account for any oxygen that had been reduced in the substrate feed while it was

not being used. Prior to feeding, a syringe containing the nutrient feed and reducing agent was

placed on the hot plate to warm to the internal temperature of the MFC for 10 minutes. Once at an

approximate temperature of 40℃, the syringe was attached to the inlet tubing of the MFC *via* a

Luer-lock connector, the MFC was tilted such that the outlet port was facing up vertically, and the

syringe was slowly emptied into the MFC, allowing any accumulated bubbles to escape.

Instructions for making the substrate feed and reducing agent may be found in the Safety and Procedures Protocol in Appendix B.

### 3.3 Continuous-flow Methodology

The continuous-flow set up consisted of several components. In congruence with the batch-fed mode, the MFC was set on top of a hot plate set at 55 ºC such that the internal temperature of the MFC could be maintained at 40 ºC. An external resistance was applied *via* a decade box, and voltage measurements were taken in parallel with the resistance using a Keithley Digital Multimeter. A 1L reservoir with nutrient feed and reducing agent added was placed upside down in a stand to allow feed to be pumped through the MFC using a low flow peristaltic pump (Cole-Parmer). The entire continuous flow set up is shown in Figure 12.
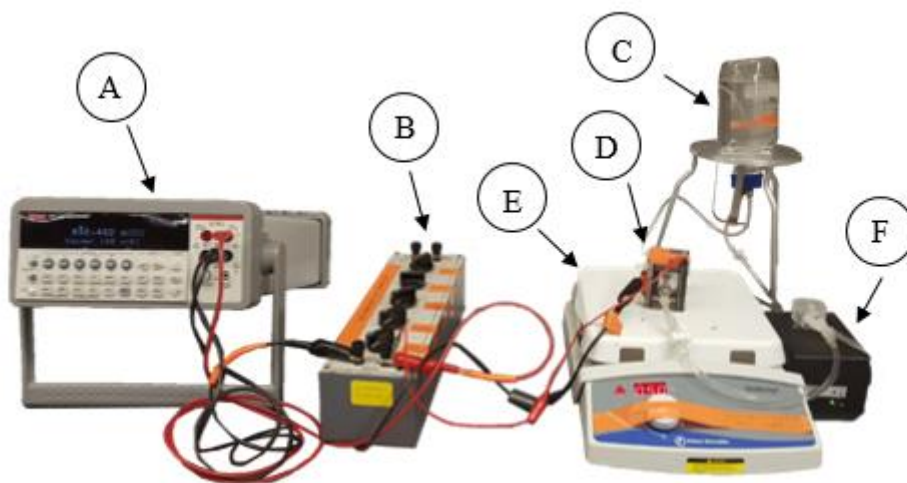


***Figure 12:*** *Continuous flow set up, including (A) Keithley Digital Multimeter, (B) Decade box, (C) 1L nutrient feed reservoir, (D) Microbial fuel cell, (E) Hot plate, (F) Peristaltic pump. Insulation is not pictured*

For each set of continuous flow measurements, a fresh 1L batch of nutrient feed was created. Prior to taking data for polarization curves, the MFC was set up in continuous-flow mode for a minimum of 6 hours to allow for settling into steady-state. The tested flow rates were 0.12 mLmin$^{-1}$, 0.21 mLmin$^{-1}$, and 0.73 mLmin$^{-1}$ and classified as low, medium, and high flow rates. In

order to obtain an idea of the inertial forces compared to the viscous forces in the MFC, the Reynolds numbers were calculated for the fuel cell using Equation 3, where it was found that, in each of the three cases, the flow was laminar:

$$Re = \frac{\rho L_c}{\upsilon} \tag{3}$$

where $\rho$ is density of the fluid in kgm$^{-3}$, $L_c$ is the characteristic length of the anode in m, and $\upsilon$ is dynamic viscosity of the fluid in Nsm$^{-2}$. Characteristic length was determined by Equation 4:

$$L_e = \frac{V_{an}}{A_{ws}} \tag{4}$$

where $L_e$ is the characteristic length in m, $V_{an}$ is the volume of the anode in m$^3$, and $A_{ws}$ is the wetted surface area in m$^2$. Another metric that is useful for comparing different MFC designs in continuous flow is Hydraulic Retention Time (HRT), which is an approximate measurement of the average amount of time that a fluid remains in a specific volume; in this case, it was how long the substrate feed stayed inside the anode chamber, in contact with the bacteria. HRT is calculated by Equation 5:

$$HRT = \frac{V_{an}}{Q} \tag{5}$$

where $V_{an}$ is the volume of the anode chamber in mL, and Q is the flow rate in mLmin$^{-1}$. Flow rates, calculated Reynolds numbers, and HRT values by anode design are shown in Table 5. It should be noted that flow rates, and, therefore, Reynolds numbers are not greatly different due to limitations of the peristaltic pump. It was found that using large tube diameters or increasing the speed for extended periods quickly wore out the motor, requiring frequent pump replacement.

*Table 5: Flow rates, Reynolds numbers, and Hydraulic Retention Time of substrate feed in the MFC for all three designs.*

| Anode Design | Q [mLmin⁻¹] | | Re | HRT [min] | HRT [h] |
|---|---|---|---|---|---|
| | $Q_{low}$ | 0.12 | 0.65 | 140.0 | 2.3 |
| Flat | $Q_{med}$ | 0.21 | 1.13 | 80.0 | 1.3 |
| | $Q_{high}$ | 0.73 | 3.94 | 23.0 | 0.4 |
| | $Q_{low}$ | 0.12 | 0.56 | 138.3 | 2.3 |
| Cones | $Q_{med}$ | 0.21 | 0.97 | 79.0 | 1.3 |
| | $Q_{high}$ | 0.73 | 3.39 | 22.7 | 0.4 |
| | $Q_{low}$ | 0.12 | 0.43 | 136.7 | 2.3 |
| Cylinders | $Q_{med}$ | 0.21 | 0.75 | 78.1 | 1.3 |
| | $Q_{high}$ | 0.73 | 2.61 | 22.5 | 0.4 |

## 3.4 Equations used for MFC Performance Analysis

Power output is a primary measure of MFC performance and is found by measuring the potential drop between the anode and the cathode of the fuel cell with an external load connected. It is given in Equation 6:

$$P = \frac{E_{MFC}^2}{R_{ext}}$$ (6)

where P is the power in W, $E_{MFC}$ is the potential drop in V, and $R_{ext}$ is the external resistance in ohms.

Power is commonly normalized to understand the efficiency with which the power is generated with the specific MFC architecture. Normalization is usually made with respect to the anode, since the anode surface area available for the biofilm to develop affects power output. Power density with normalization to the anode surface area is given in Equation 7:

$$P_{an} = \frac{E_{MFC}^2}{R_{ext}A_{an}}$$ (7)

where $P_{an}$ is the power output normalized to the anode for a power density in Wm⁻² and $A_{an}$ is the area of the wetted surface of the anode in m².

Since the practical function of MFCs lies in wastewater treatment, the physical size of the fuel cell is important to note when being designed to the application. Therefore, it is useful to know the power output with respect to the reactor volume, resulting in another form of normalization. Typically, the total chamber volume of the MFC would be accounted for, meaning both the anode and the cathode. However, the design of the MFC in this case was a single chamber air-cathode design, so only the anode chamber was used in calculating volumetric power, which is given in Equation 8:

$$P_v = \frac{E_{MFC}^2}{V_{an} R_{ext}} \tag{8}$$

Where $P_v$ is the power output normalized to the anode chamber volume for a volumetric power of $Wm^{-3}$ and $V_{an}$ is the volume of the anode main chamber ($2.28 \times 10^{-5} \text{ m}^3$) subtracting out the volume of the anode projected into it; values were shown in Table 2.

**Chapter 4: Results and Discussion**

**4.1 Batch-fed Comparison**

Before the MFC was set up in continuous-flow mode, batch-fed tests were conducted. The MFC was in batch-fed for a minimum of 3 days before switching to continuous-flow, with feeding occurring approximately once every 24 hours. In all cases, external resistance ($R_{ext}$) was at 1000 $\Omega$ and connected in parallel with the DMM, with voltage readings taken every 1 minute. Power was calculated using Equation 4. Figure 13 shows the results from batch-fed testing for the feeding period with the highest peak power output obtained out of all batch-feeding periods for each anode design. Measurements were all within 95% of peak power output.
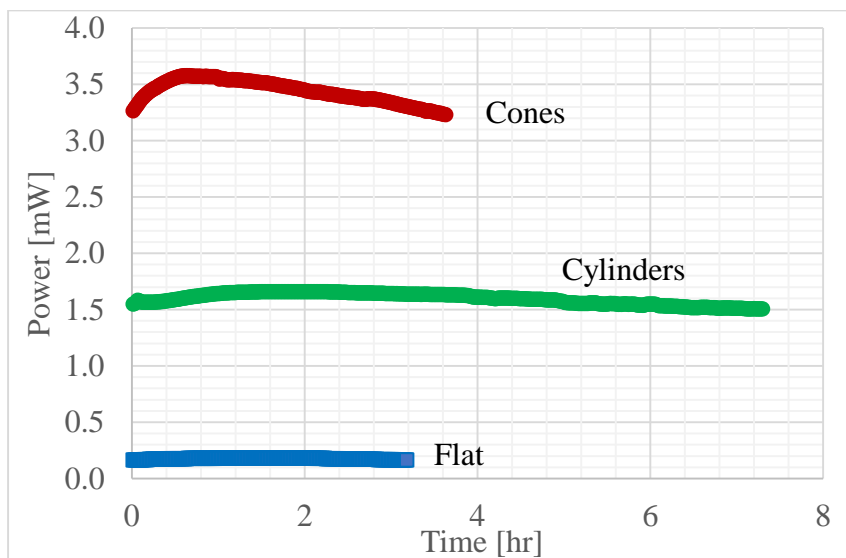


*Figure 13: Batch-fed mode data for the anode designs. Measurements were all within 95% of peak power output.*

In each batch-fed cycle, there was a linear increase to a peak output voltage and a linear decrease succeeding it. This can be best distinguished with the cones design in Figure 13. The initial positively sloped line in the power output represented the substrate conversion rate to electricity by the bacteria and the negatively sloped line represented the decreasing conversion rate [25]. Due to an initial conversion rate, peak power output was only achieved after a certain time

27

delay where the delays were 1.5 h for the flat design, 1.3 h for the cones design, and 2.0 h for the cylinders design. The slopes of these power outputs can be seen in Table 6 along with peak power output. $S_i^+$ corresponds with positive slope values, where $i$ refers to an anode design; 1 for flat, 2 for cones, and 3 for cylinders design.

*Table 6: Positive and negative slopes for one batch-fed cycle for all anode designs with corresponding $R^2$ values. Data was taken from the batch cycle that had the highest peak power output.*

| Anode Design | Peak Power Output [mW] | Positive Slope [mWh$^{-1}$] | $R^2$ | Negative Slope [mWh$^{-1}$] | $R^2$ | Time to Peak Power [h] |
|---|---|---|---|---|---|---|
| Flat | $1.8 \times 10^{-4}$ | $S_1^+ = 1.03 \times 10^{-2}$ | 0.83 | $S_1^- = -1.25 \times 10^{-2}$ | 0.98 | 1.5 |
| Cones | $3.6 \times 10^{-3}$ | $S_2^+ = 0.50$ | 0.85 | $S_2^- = -1.17 \times 10^{-1}$ | 0.99 | 1.3 |
| Cylinders | $1.7 \times 10^{-3}$ | $S_3^+ = 5.30 \times 10^{-2}$ | 0.93 | $S_3^- = -3.36 \times 10^{-2}$ | 0.98 | 2.0 |

It has been shown that steeper slopes directly correlate with larger anode sizes and greater bacteria colonization on the anode [25]. While the flat anode, which had the lowest surface area of 8.81 cm$^2$ did definitively have the lowest slope magnitudes compared to the other designs, the slopes obtained during this set of batch-fed experiments did not follow this trend of conversion rate and anode surface area precisely. The cones design had the largest magnitudes for both the positive and negative slopes at 0.50 mWh$^{-1}$ and -1.17 × 10$^{-1}$ mWh$^{-1}$, but had a smaller surface area (10.4 cm$^2$) compared to the cylinders design (13.9 cm$^2$). $R^2$ values were highest for the negative slopes, showing the strongest linear correlation was after the MFC had reached peak voltage. This was likely due to the fact that the insulation had to be removed to feed the MFC, which affected the initial conversion rates of the substrate by changing the operating temperature of the MFC [25].

The negative conversion rates did not have the same affectation as the MFC had reached steady-state temperature by that time and was not disturbed for the length of substrate depletion.

When looking at the power output in terms of density, similar trends to the slopes were seen. The peak power output from the cones design was the highest at $3.6 \times 10^{-3}$ mW compared to the cylinders and flat design, which had peak outputs of $1.7 \times 10^{-3}$ mW and $1.8 \times 10^{-4}$ mW, respectively. When normalized to the anode surface area and the anode volume, the same trends persisted, where the cones design had the largest power output, followed by the cylinders, and, lastly the flat anode design. It was reasonable that the cones and cylinder designs had larger power outputs than the flat design due to their larger surface area and closer electrode spacing (18.75 mm compared to 19.05 mm for the flat anode), although the differences here did not scale to the power output seen. The cones anode had a surface are that was 1.18 times the size of the flat anode, yet its power was 20 times greater. When comparing against the cylinders anode, the cones anode had a surface area that was smaller by a factor of 0.75 but actually had a power output 2.1 times greater than the cylinders design.

**Table 7** shows a summarization of all the results from the batch-fed mode. A possible reason for this was that the biofilm had not remained in batch-fed mode for long enough using the cylinders anode, which did not allow for proper enrichment of the bacteria and the development of a stable biofilm on the anode. This idea is explored further in Section 4.2, where this condition would also apply.

*Table 7: Batch-fed mode statistics for anode designs. Peak power densities were normalized to the wetted anode surface area and the volume of the anode chamber, respectively. Electrode space was from the top-most point of the anode. For the cones design, this was the apex of the cone.*

| Anode Design | Peak Output Power [mW] | Peak Power Density [mW/m$^2$] | Peak Power Density [mW/m$^3$] | Anode Surface Area [cm$^2$] | Electrode Spacing [mm] |
|---|---|---|---|---|---|
| Flat | $1.8 \times 10^{-4}$ | 0.27 | 10.8 | 8.81 | 19.05 |
| Cones | $3.6 \times 10^{-3}$ | 3.44 | 218.2 | 10.4 | 18.75* |
| Cylinders | $1.7 \times 10^{-3}$ | 1.19 | 101.3 | 13.9 | 18.75 |

## 4.2 Continuous-flow Comparison

Continuous-flow was followed immediately after batch-fed mode, where the MFC was initially allowed to become acclimated for a minimum of 14 hours at the lowest flow rate. As mentioned before, the flow rates used with the MFC were $Q_{low} = 0.12$ mLmin$^{-1}$, $Q_{med} = 0.21$ mLmin$^{-1}$, and $Q_{high} = 0.73$ mLmin$^{-1}$ and were tested consecutively in this order. It should be noted that the same effluent was used for all of the flow rates, meaning the substrate feed and bacteria were not replaced when a new flow rate was tested. This could have potentially changed the mixed culture composition of the MFC at each new flow rate over time, therefore affecting power output.

To compare the batch-fed results to the continuous-flow results, power output of all designs is shown in Table 8 for an external resistance set at 1000 Ω. Batch-fed peak power output values were used, and the continuous-flow power outputs were averaged from results obtained during the resistance sweep, which is discussed later. For the flat anode, it was found that the continuous-flow conditions resulted in higher power output in all flow cases, with $Q_{med}$ resulting in the highest power output of $1.04 \times 10^{-3}$ mW, a factor of 5.7 larger than the batch-fed power output. $Q_{low}$ and $Q_{high}$ had power outputs that were factors of 4.5 and 4.6 larger than the batch-fed power output. Overall, these results were expected since the advection of substrate ions to the anode and protons

to the cathode, along with the removal of waste products, is increased when the MFC is in continuous-flow mode. However, these same trends were not necessarily observed for the cones and cylinders designs. In the cones design, $Q_{high}$ had the highest power output of $3.84 \times 10^{-3}$ mW, which was a factor of 1.07 larger than the batch-fed power output of $3.58 \times 10^{-3}$ mW. $Q_{low}$ and $Q_{med}$ were shown to have power outputs that were both lower than the batch-fed power by factors of 0.95 and 0.86, respectively. In the cylinders design, this trend continued, where the highest output of $1.60 \times 10^{-3}$ mW, occurring at $Q_{low}$, was less than the batch-fed output of $1.66 \times 10^{-3}$ mW by a factor of 0.96. $Q_{med}$ and $Q_{high}$ had power outputs that were lower than the batch-fed case by factors of 0.32 and 0.51, respectively.

**Table 8:** *Batch-fed and continuous-flow power output comparison between anode designs. Power was taken at $R_{ext} = 1000$ Ω. Batch-fed power was pulled from the peak power output and continuous-flow averages were taken during a resistance sweep.*

| Anode Design | Batch-fed Power [mW] | Continuous-flow Power [mW] | | |
|---|---|---|---|---|
| | | 0.12 mLmin⁻¹ | 0.21 mLmin⁻¹ | 0.73 mLmin⁻¹ |
| Flat | $1.82 \times 10^{-4}$ | $8.26 \times 10^{-4}$ | $1.04 \times 10^{-3}$ | $8.31 \times 10^{-4}$ |
| Cones | $3.58 \times 10^{-3}$ | $3.40 \times 10^{-3}$ | $3.09 \times 10^{-3}$ | $3.84 \times 10^{-3}$ |
| Cylinders | $1.66 \times 10^{-3}$ | $1.60 \times 10^{-3}$ | $5.23 \times 10^{-4}$ | $8.45 \times 10^{-4}$ |

A possible reason for this unexpected result was that the bacteria was not enriched for long enough in batch-fed or in continuous-flow. While there is no precise enrichment or start-up period for the biofilm, a Rismani-Yazdi study in 2007 that used bovine rumen bacteria found that an average time period of 12.5 days was required for enrichment from a fresh inoculum state [19] and another study by Chen in 2008 that used wastewater had a start-up period of two months [53]. For the Pham study in 2008 that compared shear rate with power output, enrichment occurred using an empirically-determined optimal shear rate over the course of 10 days [41]. Although enrichment periods vary greatly, it is likely that the enrichment period in this study was not for a long enough

period of time, and this was due to time constraints. Therefore, there would not have been enough biofilm build up nor attachment to the anode to realize the true power output capabilities of the MFC in either batch-fed or continuous-flow mode. Regardless, a measurable power output was obtained, but future testing of this device should allow ample time for enrichment or source the bacteria from a pre-enriched inoculum to shorten the start-up period, which has also been shown to be effective [19].

**4.2.1 Polarization and Power Curves**

In order to fully characterize the MFC performance in continuous-flow mode, polarization and power density curves are used [32]. The polarization curves capture the voltage across the anode and the cathode compared to the current density, where normalization is against the wetted surface area of the anode. A linear regression curve was fitted to the polarization curve, where the cell voltage was a linear function of the current and is expressed in Equation 9:

$$E_{cell} = OCV - IR_{int} \qquad (9)$$

where $E_{cell}$ is the output voltage in V, OCV is the y-intercept and is the open circuit voltage in V, I is the current in A, and $R_{int}$ is the internal resistance in $\Omega$ and is the slope.

To generate the polarization curve, measurements were taken for varying resistances from 60 $\Omega$ to 25,000 $\Omega$ every 10 seconds for 10 minutes at pseudo steady-state. Pseudo steady-state was determined as the point where percent deviation between measurements taken from start to stop was less than 5%. Measurements started at 1000 $\Omega$, were stepped up 25,000 $\Omega$, went back down to 60 $\Omega$, and finally came back up to 1000 $\Omega$. This was done to account for hysteresis in the data. The voltages were averaged at each resistance and used in the polarization curve.

The power curves capture the power density compared to the current density. From this curve, the Maximum Attainable Power Density (MAPD) is taken, which is a common metric used

to compare MFCs against each other [32] and will be used to compare the anode designs here. Additionally, the external resistance at the MAPD is approximately equivalent to the internal resistance of the MFC [32], and this was also recorded.

## 4.2.2 Design Comparisons for Variable Flow Rates

In order to compare the results in a manner that aligns with the intent of this thesis, the three anode designs are first compared at each flow rate. In Section 4.2.2., flow rates are compared for each design and are given in a more abridged version since the same set of data is presented but in a different format. A summary table of all results from the polarization curve can be seen in Table 9, and the summary table for the power curve results can be seen in

**Table 10**.

The first flow rate tested was the low flow rate ($Q_{low}$) at 0.12 mL·min$^{-1}$. Polarization and power curves are shown in Figures 9 and 10, respectively. The cones design had the highest OCV at 187 mV. Open circuit voltage of the flat design was second highest at 127 mV the cylinders design had the lowest OCV of 146 mV. In terms of internal resistance determined by the slope of the fitted linear regression curve, the cones had the lowest $R_{int}$ at 2.29 kΩ, followed by the flat design at 3.17 kΩ, and, lastly, the cylinders design at 3.69 kΩ. Linear-regression curves were considered to be good fits, as all $R^2$ values were 0.95 or above.

34

**Figure 14:** *Polarization curve of anode designs at $Q_{low} = 0.12$ mL·min$^{-1}$. Lines of best fit are shown. Standard error bars are shown but are too small to be viewed with respect to the size of the plotted points.*

Corresponding to the polarization curve (**Figure 1**Figure 15), the cones design had the highest MAPD out of the three designs at 3.75 mWm$^{-2}$. Compared to the flat design of 1.09 mWm$^{-2}$ and the cylinders design MAPD of 1.48 mWm$^{-2}$, the cones design MAPD was larger by factors of 3.44 and 2.53, respectively. From high to low, the order of MAPD output based on design was cones, cylinders, and, lastly, flat design. This also correlated with the internal resistance as expected, whereby a lower resistance resulted in higher power output. As mentioned in Section 4.3, the internal resistance of the fuel cell is equivalent to the external resistance at MAPD. Based on the resistance sweep, the cones design was found to have an experimental internal resistance of 1759 Ω, $R_{int}$ of the cylinders design was 2656 Ω, and $R_{int}$ of the flat design was 3798 Ω. It was observed that the experimental $R_{int}$ for each case had large deviations from the calculated $R_{int}$, ranging from 19.9% to 28.1% in difference. Since the MFC experienced large internal resistances, a higher resolution of tested resistances would be required in order to obtain closer resistances to what was calculated.

35

*Figure 15: Power curve of anode designs at $Q_{low}$ = 0.12 mL·min$^{-1}$. Standard error bars are shown but are too small to be viewed with respect to the size of the plotted points.*

The next flow rate tested was at 0.21 mLmin$^{-1}$, and the polarization curve can be seen in Figure 16. In this stage, the cones design still had the highest OCV at 183 mV, followed by the flat design OCV of 117 mV, and finally the cylinder design OCV of 145 mV. Internal resistances were comparable to those obtained at $Q_{low}$ for the cones design, which was calculated to be 2.32 kΩ. The flat anode had a slightly lower internal resistance than at $Q_{low}$ of 2.42 kΩ. However, the cylinders anode internal resistance was more than twice what was obtained previously, resulting in an internal resistance of 7.71 kΩ. This limited the power output, as is observed in the power curve (Figure 17). Similar to the polarization curve at $Q_{low}$, high $R^2$ values of 0.98 or greater meant that the OCV and $R_{int}$, or the y-intercept and slope of the line, were a good linear fit to the experimental data.
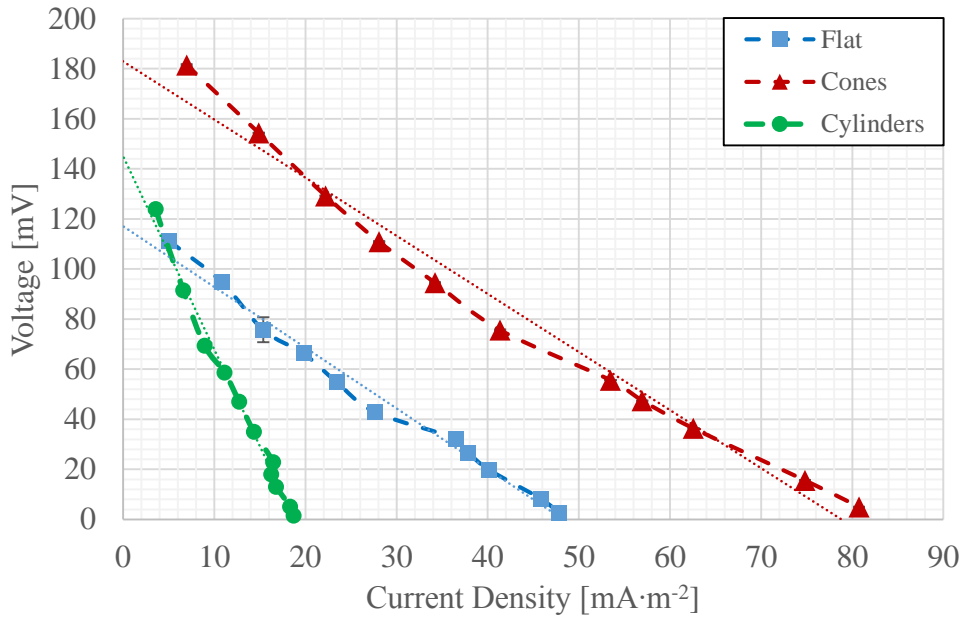
**Figure 16:** *Polarization curve of anode designs at $Q_{med} = 0.21$ mL·min$^{-1}$. Lines of best fit are shown. Standard error bars are shown.*

In observing the power curve (Figure 17), the differences between power outputs at $Q_{low}$ and $Q_{med}$ became more apparent. While the cones anode still held the highest MAPD at 3.23 mWm$^{-2}$, the flat anode had the second highest output at 1.31 mWm$^{-2}$, with the cylinders anode at the lowest MAPD of 0.65 mWm$^{-2}$. Compared to the flat and cylinders anodes, the cones MAPD was higher by a factor of 2.47 and 4.97, respectively. Between $Q_{low}$ and $Q_{med}$, the scaling factor between the cones and cylinders designs doubled, primarily due to the cylinders design having a lower MAPD that did not scale with the increased flow rate. Possible reasons for this are discussed in Section 4.2.3, where all flow rates are evaluated for each anode design. Observing the experimental internal resistances, the cones design had the lowest at 2656 Ω while the flat and cylinders designs had values of 3798 Ω.
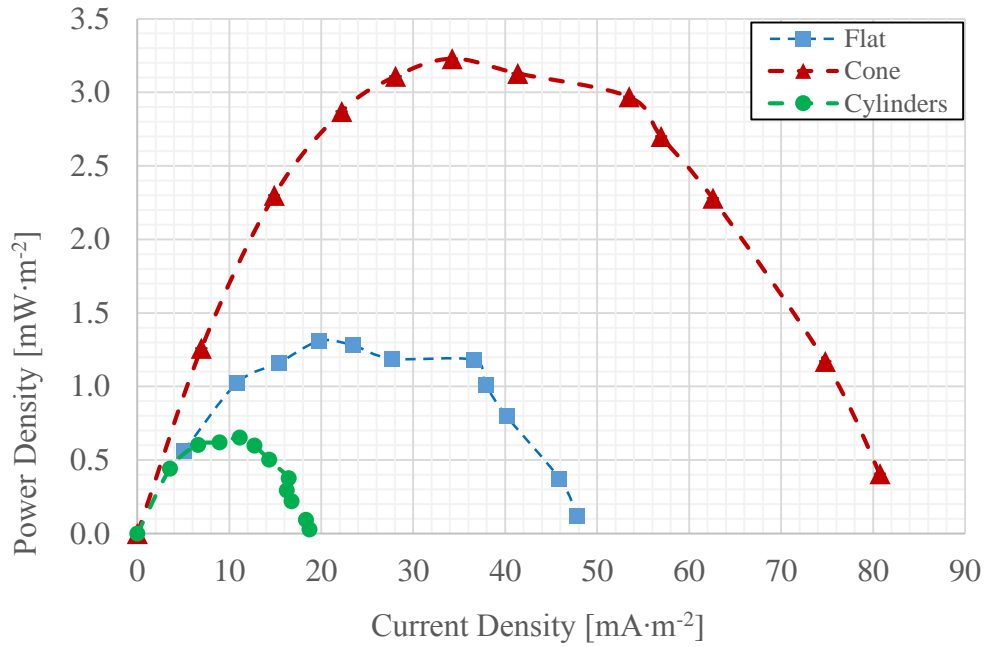
***Figure 17:*** *Power curve of anode designs at $Q_{med}$ = 0.21 mL·min$^{-1}$. Standard error bars are shown but are too small to be viewed with respect to the size of the plotted points.*

The high flow rate of 73 mLmin$^{-1}$ had similar trends to that of the medium flow rate. Again, the cones design had the highest OCV at 153 mV, which was followed by the cylinders design OCV of 146 mV, and, lastly, the flat design OCV of 108 mV. The cones anode again had the lowest internal resistance at 1.48 kΩ. The flat anode followed next with $R_{int}$ calculated to be 2.37 kΩ. The cylinders anode again had the highest internal resistance, calculated to be 5.83 kΩ. Like the previous two flow rates, the $R^2$ values were high at 0.98 or greater, meaning that these obtained values were a good linear fit to the experimental voltages obtained from the resistance sweep. The polarization curve can be seen in Figure 18.
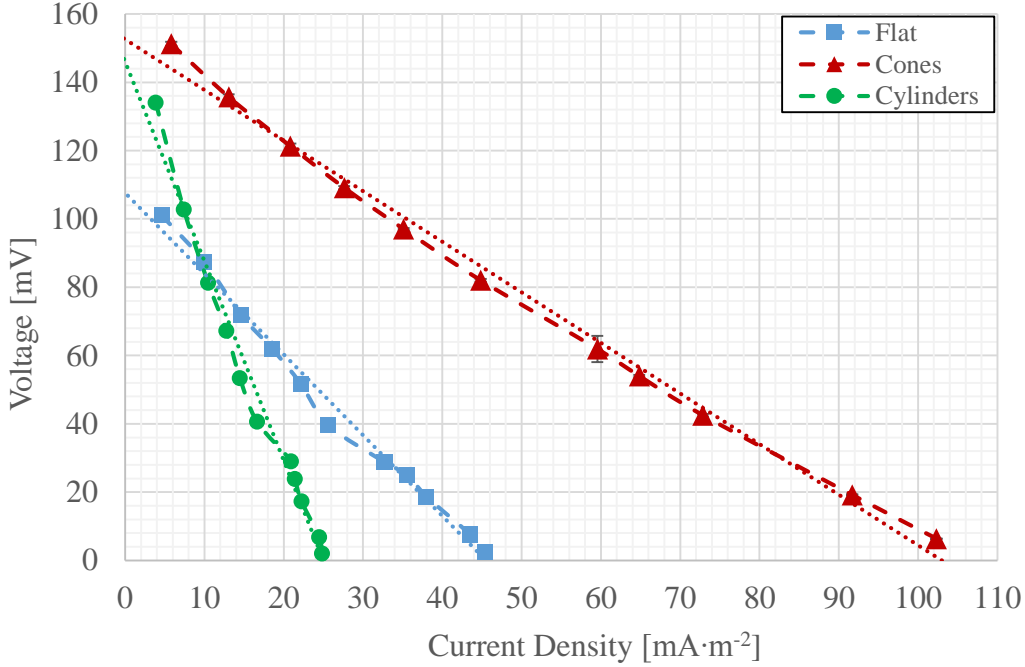
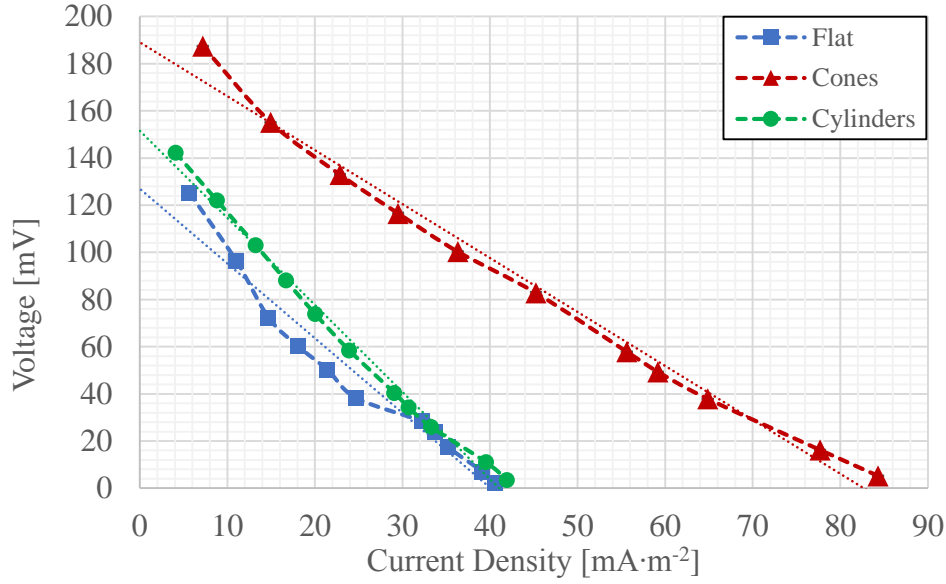**Figure 18:** *Polarization curve of anode designs at $Q_{high}$ = 0.73 mL·min$^{-1}$. Lines of best fit are shown. Standard error bars are shown but are too small to be viewed with respect to the size of the plotted points.*

Figure 19 shows the power curve for the high flow rate of 0.73 mLmin$^{-1}$. The cones design had the highest MAPD at 3.69 mWm$^{-2}$, followed by the flat design at 1.15 mWm$^{-2}$, and, lastly, the cylinders design at 0.86 mWm$^{-2}$. This meant that the cones had an MAPD with a factor of 3.21 greater than the flat anode and a factor of 4.29 greater than the cylinders anode. While the scaling factor for the flat anode at the high flow rate was comparable to the scaling factor at $Q_{low}$ (factor of 3.44), the cylinders scaling factor remained high at 1.70 times greater than the low flow scaling factor. This further supported the idea that the cylinders power output did not scale with the increasing flow rate. Experimental internal resistance was lowest for the cones design at 1000 $\Omega$, while the flat and cylinders designs were again both at 3798 $\Omega$, and 3798 $\Omega$, respectively.
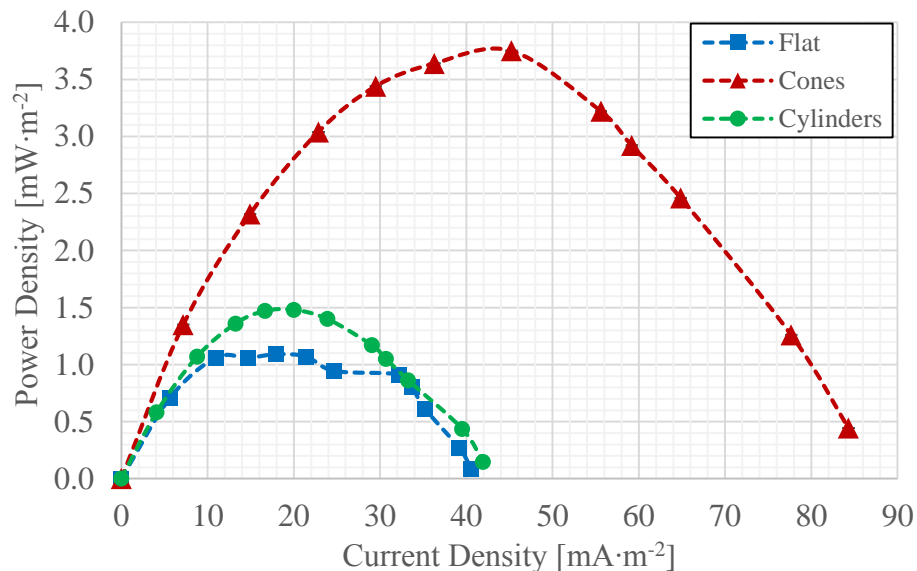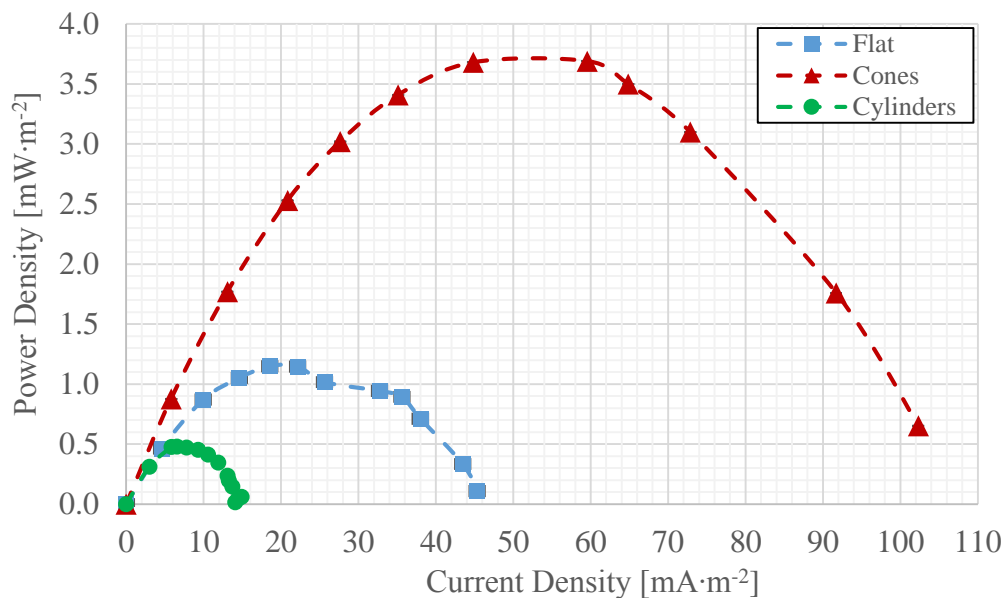
***Figure 19:*** *Power curve of anode designs at $Q_{high}$ = 0.73 mL·min$^{-1}$. Standard error bars are shown but are too small to be viewed with respect to the size of the plotted points.*

To summarize, several trends were observed when comparing anode designs at each individual flow rate. $R^2$ values were high for all polarization curves, indicating a close fit of the linear-regression curve to the experimental data. However, calculated internal resistances from the slopes of the regression curves did not correlate well with the experimentally-determined internal resistances that were found at MAPD, where percent deviation from the calculated $R_{int}$ ranged from 14.4% to as much as 60.6%. This was due to the internal resistance of the MFC being very large, such that a finer resolution of tested resistances would be needed to determine a more accurate $R_{int}$. As a result of these high internal resistances, power output of the MFC in this study was low in comparison to other MFCs found in literature, and power densities using different anode geometries are only comparable relative

It was observed that the highest MAPD and lowest internal resistance was found for the cone design at all flow rates. Based on this, the cylinders design should be selected for future design considerations in microbial fuel cells. Observing the other designs, at $Q_{low}$, the cylinders

design had a higher MAPD than the flat design, but the flat design overtook the cylinders design and achieved higher MAPDs at $Q_{med}$ and $Q_{high}$. This suggests that, despite the fact that the cylinder had a larger surface area than the flat anode, its surface geometry may have, in fact, interfered with its ability to produce a higher output than the flat anode. This idea will be explored further in Section 4.2.3, where anode designs are individually analyzed under the three flow rate conditions. Quantified summaries of all three designs and all relevant data from the polarization and power curve plots can be found in Table 9 and

**Table 10**, respectively.

*Table 9: Summarization of polarization curve data for all anode designs. Internal resistance ($R_{int}$) and open current voltage (OCV) were determined from a linear regression curve fitted to the data.*

| Anode Design | Flow Rate [mL·min$^{-1}$] | Slope, $R_{int}$ [kΩ] | R$^2$ | OCV [mV] |
|---|---|---|---|---|
| Flat | 0.12 | 3.17 | 0.95 | 127 |
| | 0.21 | 2.42 | 0.99 | 117 |
| | 0.73 | 2.37 | 0.99 | 108 |
| Cones | 0.12 | 2.29 | 0.99 | 189 |
| | 0.21 | 2.32 | 0.98 | 183 |
| | 0.73 | 1.48 | 0.99 | 153 |
| Cylinders | 0.12 | 3.69 | 0.99 | 152 |
| | 0.21 | 7.71 | 0.99 | 145 |
| | 0.73 | 5.83 | 0.98 | 146 |

*Table 10: Summarization of power curve data for all anode designs. Percent difference was taken between the experimentally-determined internal resistance and the calculated internal resistance based on the slope of the polarization curve.*

| Anode Design | Flow Rate [mL·min$^{-1}$] | MAPD [mW/m$^2$] | $R_{ex}$ at MAPD [kΩ] | Power Density at Rex = 1 kΩ [mW/m$^2$] | $R_{int}$ [kΩ] | Percent Difference [%] |
|---|---|---|---|---|---|---|
| | 0.12 | 1.09 | 3798 | 0.944 | 3168 | 19.9% |
| Flat | 0.21 | 1.31 | 3798 | 1.18 | 2422 | 56.8% |
| | 0.73 | 1.15 | 3798 | 0.943 | 2365 | 60.6% |
| | 0.12 | 3.75 | 1759 | 3.22 | 2288 | 23.1% |
| Cones | 0.21 | 3.23 | 2656 | 2.97 | 2321 | 14.4% |
| | 0.73 | 3.69 | 1000 | 3.69 | 1481 | 32.5% |
| | 0.12 | 1.48 | 2656 | 1.17 | 3693 | 28.1% |
| Cylinders | 0.21 | 0.65 | 3798 | 0.376 | 7713 | 50.8% |
| | 0.73 | 0.86 | 3798 | 0.608 | 5836 | 34.9% |

### 4.2.3 Flow Rate Comparisons

Since separate polarization and power curves were already plotted comparing designs in the previous section, polarization and power curves are plotted here on the same graph for brevity. Additionally, a summary table showing scaling factors between max MAPD and other MAPD values is shown in Table #. For the baseline flat design, comparison amongst the three flow rates showed the lowest MAPD collected was 1.09 mWm$^{-2}$ at $Q_{low}$. Immediately following that, the highest MAPD value was obtained at $Q_{med}$ at 1.31 mWm$^{-2}$. At $Q_{med}$, the MAPD dropped down to 1.15 mWm$^{-2}$. From this, it could be deduced that there exists some threshold where some optimal flow rate exists for a maximum power output. While this is a possible conclusion, this would also need to be consolidated with previous work that has shown that an increase in shear rate results in higher power output [41]. Further testing at flow rates both in between $Q_{med}$ and $Q_{high}$ as well as

42

higher flow rates would be necessary in order to draw a firm conclusion on this. The polarization and power curves can both be seen in Figure 20.

There were also some noticeable inconsistencies with the power curve, where the inverted parabola did not follow a smooth parabolic shape and, instead, had some "waviness" to it. As subsequent power curves for the cylinder and cone designs do not experience this same issue, it is more likely that there was some error in data collection, where the voltage dataset captured was not all within the pseudo steady-state condition. This appeared to be particularly true for the data points plotted at 26 mAm$^{-2}$. However, because standard error bars for power density did not intersect at MAPD for any of the tested flow rates, the differences here were still considered statistically significant. A repeated test for this trial with ample time allowed for settling into pseudo steady-state would be necessary in order to generate smoother polarization and power curves.

***Figure 20:*** *Polarization and polar curves of the flat design at the low, medium, and high flow rates. Standard error bars are plotted but are too small with respect to the plotted points.*

For the cones design, maximum MAPD occurred at the lowest flow rate at a value of 3.75 mWm$^{-2}$. However, this was larger than the next highest MAPD (3.69 mWm$^{-2}$) by just a factor of 1.02, which occurred at the highest flow rate. The max MAPD was larger than the lowest MAPD (3.23 mWm$^{-2}$) by a factor of 1.16. Since the two highest MAPD values were very similar to each other and occurred at the lowest and highest tested flow rates in this experiment, no conclusive trend could be discerned from the plotted curves (Figure 21). Due to the fact that the cones design had the highest power output, it would be worthwhile to test higher flow rates for future work and determine an optimal shear rate, such that this could be compared to a flat anode at its optimal power output. The flow rates in this study resulted in Reynolds numbers less than 4, so it is likely that, while the low inertia, highly viscous flow was able to provide a constant stream of fresh

44

substrate and nutrients to the bacteria, it did not allow the MFC to perform at its full capabilities.

Table 11 reproduces the Reynolds numbers for all anode designs at each flow rate for convenience.

Figure 21 shows the polarization and power curves for the cones anode design.

**Table 11:** *Anode designs at all flow rates with corresponding Reynolds numbers.*

| Anode Design | Q [mLmin$^{-1}$] | | Re |
|---|---|---|---|
| | $Q_{low}$ | 0.12 | 0.65 |
| Flat | $Q_{med}$ | 0.21 | 1.13 |
| | $Q_{high}$ | 0.73 | 3.94 |
| | $Q_{low}$ | 0.12 | 0.56 |
| Cones | $Q_{med}$ | 0.21 | 0.97 |
| | $Q_{high}$ | 0.73 | 3.39 |
| | $Q_{low}$ | 0.12 | 0.43 |
| Cylinders | $Q_{med}$ | 0.21 | 0.75 |
| | $Q_{high}$ | 0.73 | 2.61 |
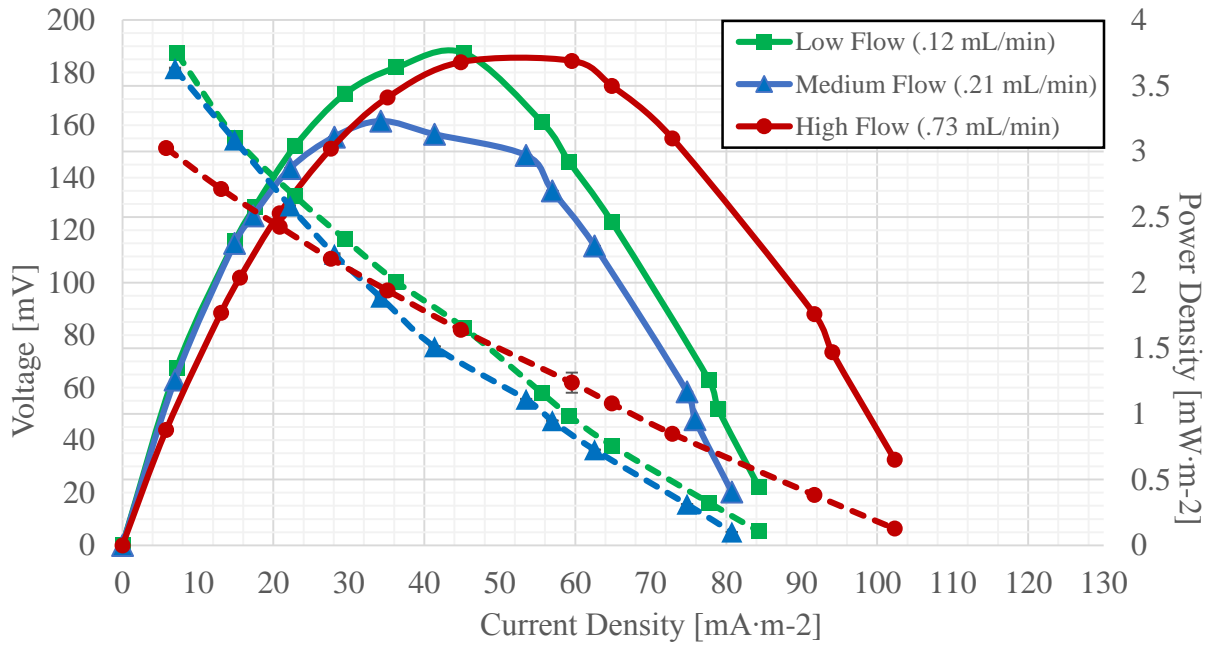


**Figure 21:** *Polarization and polar curves of the cone design at the low, medium, and high flow rates. Standard error bars are plotted but are too small with respect to the plotted points.*

For the cylinders design, the low flow rate had undoubtedly the largest MAPD and overall power output at 1.48 mWm$^{-2}$. The largest MAPD scaled the next highest and lowest MAPD's by 1.72 and 2.28, respectively, which were very large compared to previous designs. The second

highest MAPD (0.86 mWm$^{-2}$) occurred at Q$_{high}$ while the lowest MAPD (0.65 mWm$^{-2}$) occurred at Q$_{med}$. To explain these trends, Reynolds numbers may again be examined. At Q$_{low}$, the Re value was only 0.43. Since it was so low, it is possible that, although substrates were being effectively delivered to the anode and oxidized by the bacteria, this was not a high enough flow rate to cause shearing at the anode. Thus, during this stage of testing, the biofilm may have only accrued some mass. Furthermore, without a proper enrichment time length, the larger flow rates of Q$_{med}$ and Q$_{high}$ could have sheared off fragments of biofilm, thus decreasing power output.
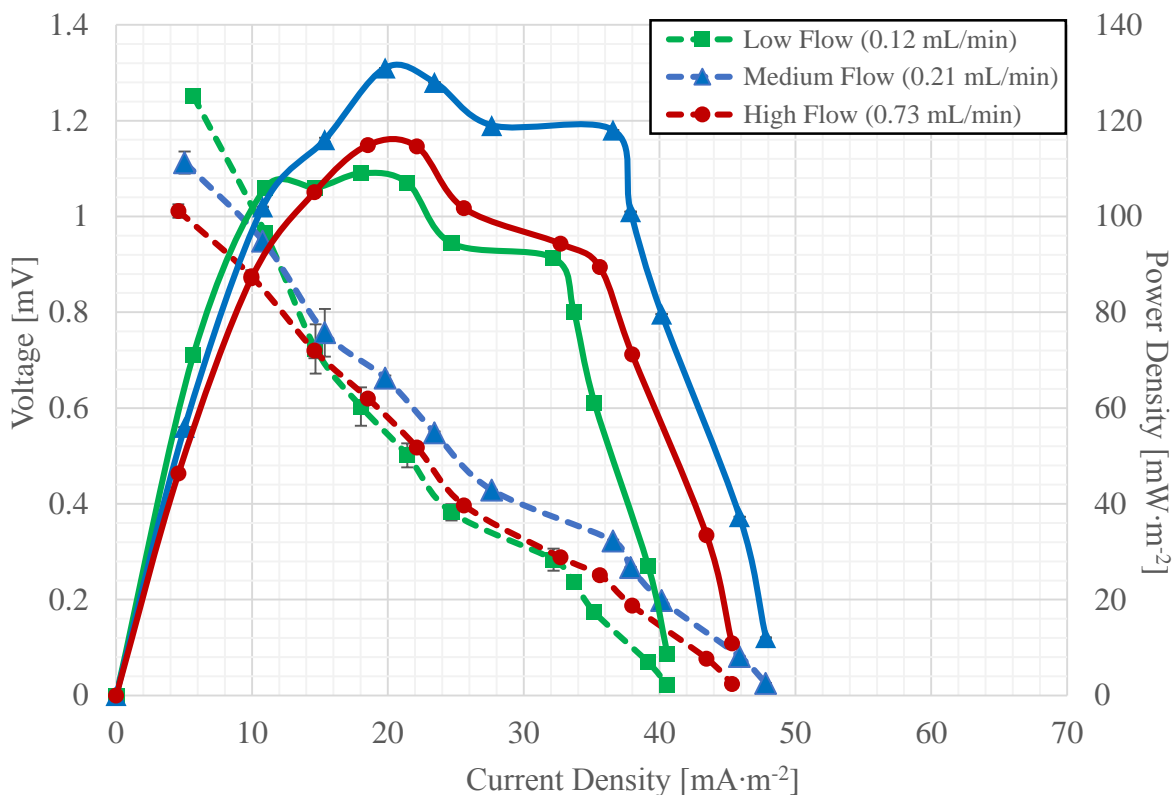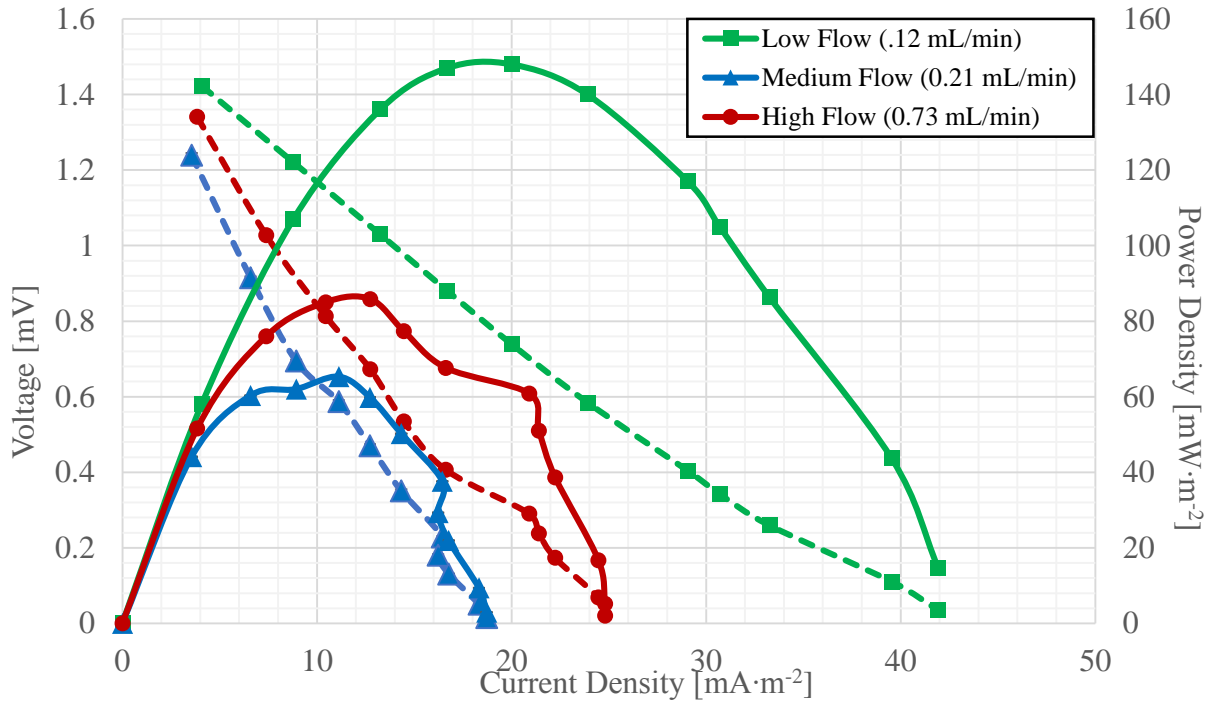


*Figure 22: Polarization and polar curves of the cylinder design at the low, medium, and high flow rates. Standard error bars are plotted but are too small with respect to the plotted points.*

Another possible limitation that could explain the decrease in power output for the cylinders design would be the velocity gradients and streamlines that developed according to the anode geometry. As was mentioned in the previous work with this MFC, it is possible that recirculation regions that existed in the anode chamber limited the diffusion regime of substrate and vital nutrients, therefore limiting power output. For convenience, Figure 6, which shows the

velocity gradient and streamlines, is reproduced here as Figure 23. Recirculation would have simultaneously prevented waste products and hydrogen ions from being removed while also
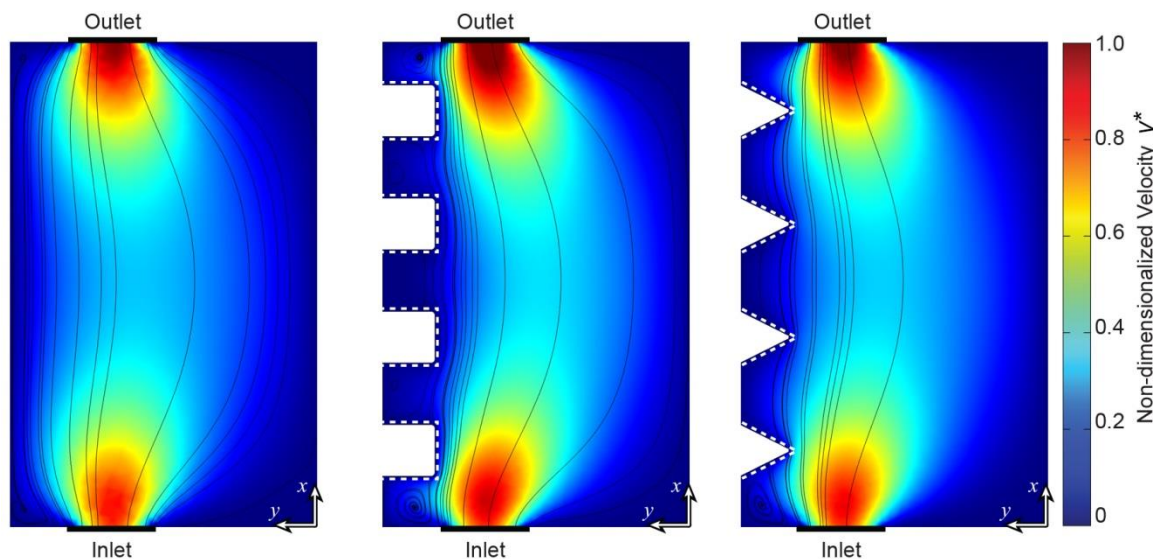


***Figure 23:*** *Velocity plots of (a) flat, (b) cylinder, and (c) cone designs in a 2D cross section showing the side profile of the MFCs. Streamlines are indicated with black lines for the x and y components of velocity, which is non-dimensionalized* [25].

keeping fresh substrate from reaching the bacteria to be oxidized. While all three designs exhibited these regions near the inlet and outlet, the cylinders design exhibited these between almost every single structure. As a result, a biofilm would have only been able to form on or near the top facets of the cylinder structures, resulting in a surface area reduction to approximately 9% of the original. This would have severely limited the power output in the cylinder design and is a possible explanation for the power drop at higher flow rates.

In summary, the power densities collected at variable flow rates resulted in different trend observations for all anode designs. For the flat anode, the highest MAPD occurred at the medium flow rate followed by the lowest MAPD at the high flow rate, indicating the possible existence of a threshold for flow rate between $Q_{med}$ and $Q_{high}$, which, upon reaching, would result in the largest MAPD achievable for the flat anode. This would require further testing at flow rates in between $Q_{med}$ and $Q_{high}$. For the cones anode, there was no conclusive trend as the low and high flow rates

had similar MAPDs with the minimum MAPD occurring at the medium flow rate, so it would be recommended to test this anode design at higher flow rates to determine a conclusive trend. The cylinders anode had its highest MAPD at the low flow rate with a steep drop off at the medium and high flow rates. This was attributed to recirculation areas that might have developed more fully at the medium and high flow rates. Summaries of the MAPD results with respect to the flow rate can be found in Figure 24 and a table quantifying the highest MAPD relative to the lower MAPDs can be seen in Table 12.
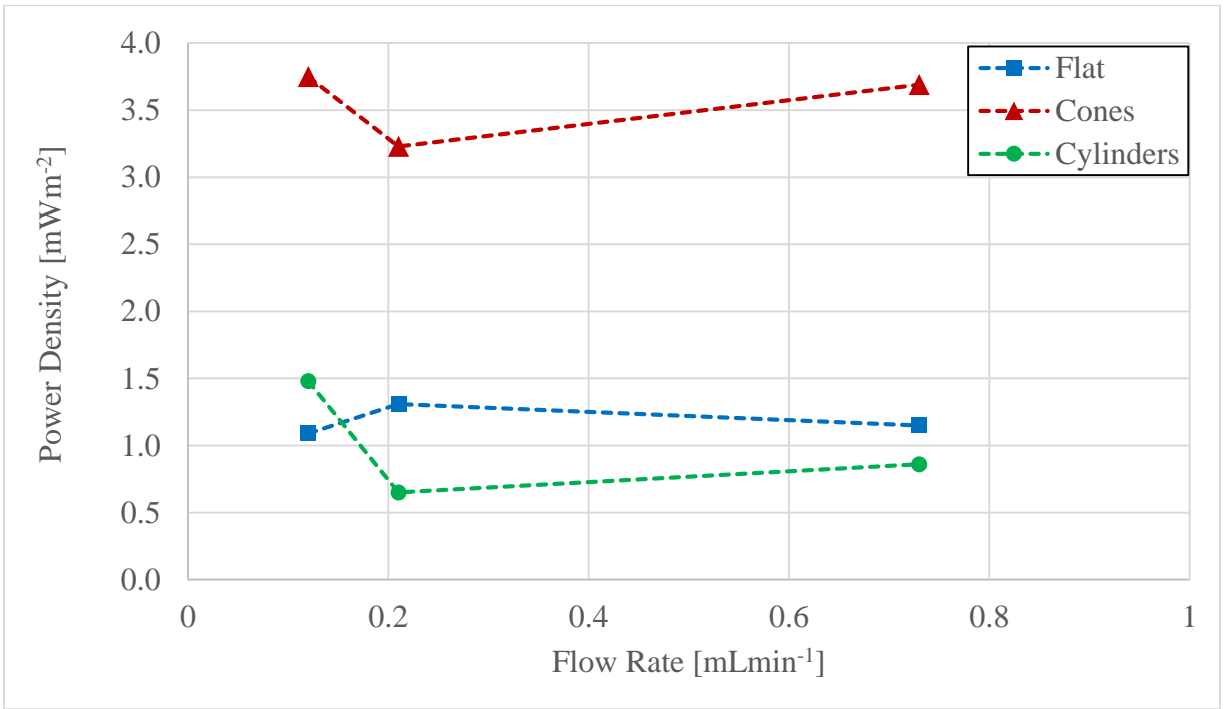


*Figure 24: Anode design maximum attainable power densities as a function of flow rate.*

*Table 12: Summary table of flow rate comparisons for each anode design. $Q_1$ is the flow rate at which the highest MAPD was found, and subsequent scaling factors are calculated based off of the MAPD at $Q_1$.*

| Anode Design | Max MAPD [mWm$^{-2}$] | $Q_1$ [mLmin$^{-1}$] | $\dfrac{MAPD_{Q_1}}{MAPD_{Q_2}}$ | $\dfrac{MAPD_{Q_1}}{MAPD_{Q_3}}$ |
|---|---|---|---|---|
| Flat | 1.31 | Med | $\dfrac{\text{High}}{1.14}$ | $\dfrac{\text{Low}}{1.2}$ |
| Cones | 3.75 | Low | High | Med |

| | | | 1.02 | 1.16 |
|---|---|---|---|---|
| | | | High | Med |
| Cylinders | 1.48 | Low | 1.72 | 2.28 |

## 4.3 Error Mitigation

Although some of the low power output from the MFC can be explained based on fluid dynamics and physics theory, a larger potential influence on the continuous-flow mode resulted in issues with the experiment. During the cones and cylinders continuous-flow testing, both MFCs leaked. This was likely due to cyclic loading wearing down on the graphite anode when compressed together with the rest of the MFC assembly using the nylon screws and nuts. This primarily occurred for one or two days after start up, and retightening the nuts on new, unused bolts was the solution for this issue. Applying heat to the acrylic anode chamber and anode end plate while compressing them may have also caused these parts to distort, further increasing the likelihood of MFC leakage. As a result, there is a possibility that oxygen leaked into the anode chamber, which would have decreased overall power output. Although it is also possible that the reducing agent was able to eliminate this oxygen, a more detailed analysis would need to be conducted to see if it was expended entirely. Due to time limitations, these experiments were unable to be performed with newly machined MFC parts. In the future and as general best practice, it would be recommended to have several MFC spare parts at hand in case another part fails.

**Chapter 5: Summary and Conclusions**

**5.1 Contributions to the MFC Field**

Through this thesis work, a single chamber, air-cathode microbial fuel cell that was capable of implementing three different anode types (flat, patterned cones, and patterned cylinders) was fabricated and characterized. Safety protocol and testing methodology was also developed for the experiment, which can be found in Appendix B.

For all designs, the MFC was first tested in batch-fed mode, which was followed by continuous-flow mode at three different flow rates: $Q_{low}$ was 0.12 $mLmin^{-1}$; $Q_{med}$ was 0.21 $mLmin^{-1}$; and $Q_{high}$ was 0.73 $mLmin^{-1}$. It was observed that, in batch-fed, the cones design had the highest peak power density at 3.44 $mWm^{-2}$. Since the cones design had a smaller surface area compared to the cylinders design, it was likely that the enrichment period for the bacteria was not long enough. In a quiescent fluid, power output should have been primarily dependent on surface area. Transitioning between batch-fed to continuous-flow, it was found that the flat anode was the only design to achieve higher power output at the continuous-flow feeding mode. From Section 4.3, it was determined that a probable cause for this was due to the fact that the MFC leaked with the cones and cylinders designs as a result of wear and fatigue from repeated cyclic loadings on the MFC parts. This would have introduced oxygen into the anode chamber of the MFC, decreasing power output.

In continuous-flow mode, despite the early leakage, the cones design still had the highest power density output at all flow rates. While the cylinders design had the second highest MAPD at $Q_{low}$, the flat anode overtook the cylinders design in MAPD output at $Q_{med}$ and $Q_{high}$. This was likely due to a combination of a short biofilm enrichment period of less than five days as well as recirculation that developed in the anode chamber with the cylinders design [25]. Due to this, the

cylinders design should be rejected from further considerations for an anode design. Moving forward, the cones design should be considered for future MFC designs as its increased surface area and structural geometry allow it to generate higher power relative to a flat anode made from the same graphite material. In testing the patterned $4 \times 4$ array of cones, it would also be helpful to continue using a flat anode as a baseline comparison until this geometry and resulting power output are well-understood at a large range of flow rates.

**5.2 Future Work**

Although the patterned cylinders anode is the apparent choice anode design, additional studies must be conducted to make a more informed decision. On the subject of flow rates, it is necessary to test additional flow rates between $Q_{med}$ and $Q_{high}$; the reason for this is because it appeared as though the flat anode had some optimal shear rate that would allow for an absolute maximum MAPD. Flow rates above $Q_{high}$ should also be tested in the future, as the cones design did not have conclusive trends based on the highly viscous flow rates that were selected for this study.

Future work would also involve taking a more detailed look into the microbial community of the MFC. When testing different flow rates, new bacteria was not inoculated into the MFC in between different flow rates. Therefore, it is possible that the bacterial composition and density of the MFC changed over time as a function of both surface area and surface geometry. To determine if this is true, a denaturing gradient gel electrophoresis (DGGE) study should be conducted to observe the existing bacterial species within the fuel cell. Along these same lines, it would be useful to understand how thick the biofilm becomes under different flow rate conditions as well as where it is thickest. Anodes should be analyzed with scanning electron microscopy, and this would

likely help explain some of the loss of power seen when the cylinders design was implemented in the MFC.

In order to make this study more comparable to other MFC designs, it would be useful to have greater power output. One easily implemented method would be to increase the bacteria concentration within the MFC, since a concentration of just 1% v/v was used for inoculation in this study. A higher concentration of bacteria might result in better extracellular electron-transferring abilities and a thicker biofilm early on. Another means of increasing power output would be to lower the cathode over-potential. As mentioned in Chapter 2, the thick graphite plate led to low mass diffusivity of oxygen, which increased MFC internal resistance. If a thinner material were chosen with a greater surface area in contact with oxygen, power output would likely be improved.

While the future of MFCs is bright, there are still several shortcomings in the field. Problems such as understanding the interactions of a mixed culture inoculum in direct interspecies electron transfer, reducing internal loss through electrode material and geometry design decisions, and engineering the internal fluid flow dynamics all must be well-understood– first at a research laboratory scale, and, eventually, at a scale worthy of practical application, where MFCs would ideally be implemented in wastewater treatment centers. Although the path may be long, optimizing this carbon-neutral form of alternative energy is a step in the right direction and could serve to benefit society on a global scale.

## References

[1]     X. Lemaire, *Glossary of Terms in Sustainable Energy Regulation* [Online], Available: http://www.reeep.org/sites/default/files/Glossary%20of%20Terms%20in%20Sustainable%20Energy%20Regulation.pdf

[2]     F. Birol, et. al. (2015). *World Energy Outlook 2015 Factsheet* [Online]. Available: http://www.worldenergyoutlook.org/media/weowebsite/2015/WEO2015_Factsheets.pdf

[3]     N. Abas, A. Kalair, N. Khan, "Review of fossil fuels and future energy technologies," *Futures*, 69: 31-49, May 2015.

[4]     V. Ramanathan, Y. Feng, "Air pollution, greenhouse gases, and climate change: Global and regional perspectives," *Atmospheric Environment*, vol 43, pp. 37-50, 2009.

[5]     Institute for Energy Research. (2015). *Fossil Fuels* [Online]. Available: http://instituteforenergyresearch.org/topics/encyclopedia/fossil-fuels/?

[6]     U.S. Energy Information Administration, *Annual Energy Outlook 2015*, 2015.

[7]     M. Maupin, et al., "Estimated Use of Water in the United States in 2010: U.S. Geological Survey," U.S. Department of the Interior, Reston, VA, 2014.

[8]     M. Paque, et al., "Ground Water Report to the Nation: A Call to Action," Ground Water Protection Council, 2007.

[9]     U.S. Geological Survey. (2016 February 19). *Drought Impacts* [Online]. Available: http://ca.water.usgs.gov/data/drought/drought-impact.html

[10]    M. Sophocleous, "Conserving and extending the useful life of the largest aquifer in North America: The future of the High Plains/Ogallala Aquifer," *Groundwater,* vol. 50, pp. 831–839, 2012.

[11]    B. Virdis, et. al., *Microbial Fuel Cells*, pp. 641-664, 2011.

[12]   *Irrigation Water Management: Training Manual No. 6 - Scheme Irrigation Water Needs and Supply*, 6th ed., Food and Agriculture Organization of the United Nations, 1992, Ch. 2.1.1.

[13]   National Research Council of the National Academies, "Water Reuse: Potential for Expanding the Nation's Water Supply Through Reuse of Municipal Wastewater," The National Academies Press, Washington, D.C., 2012.

[14]   M.A. Shannon, et al., "Science and technology for water purification in the coming decades," *Nature, vol.* 452, pp. 301–310, 2008.

[15]   *Notes on Activated Sludge Process Control*, State of Maine Department of Environmental Protection, MN, 2009, pp. 3 – 19.

[16]   "Energy Efficiency in Water and Wastewater Facilities," U.S. Environmental Protection Agency, Washington, D.C., May 2013.

[17]   "February 2016: Monthly Energy Review," U.S. Energy Information Administration, Washington, D.C., 2016.

[18]   Z. Du, et al, "A State of the art review on microbial fuel cells: A promising technology for wastewater treatment and bioenergy," *Biotech Advances*, vol 25, pp. 464-482, 2007.

[19]   H. Rismani-Yazdi, et al., "Electricity Generation from Cellulose by Rumen Microorganisms in Microbial Fuel Cells," *Biotechnology and Bioengineering*, vol.97, pp.1398-1407, 2007.

[20]   H.J. Kim, et al., "A mediator-less microbial fuel cell using a metal-reducing bacterium, *Shewanella putrefaciens*," *Enzyme and Microbial Technology*, vol. 30, pp.145-152, 2002.

[21] B.H. Kim, et al., "Direct electrode reaction of Fe(III)-reducing bacterium, *Shewanella putrefaciens*," *Journal of Microbiology and Biotechnology*, vol. 9, pp. 127-131, 1999.

[22] K. Rabaey, et. al., "Microbial phenazine production enhances electron transfer in biofuel cells," *Environmental Science & Technology*, vol. 39, pp. 5373-5382, 2005.

[23] D.R. Bond, D.R. Lovley, "Electricity production by *Geobacter sulfurreducens* attached to electrodes," *Applied Environmental Microbiology*, vol. 69, 1548-1555, 2003.

[24] G. Reguera, et al., "Extracellular electron transfer via microbial nanowires," *Nature*, vol. 435, pp. 1098-1101, 2005.

[25] M. Gerber, "The Effect of Anode Geometry on Power Output in Microbial Fuel Cells," M.S. Thesis, Dept. Mech. and Aero. Eng., Ohio St. Univ., Columbus, OH, 2014.

[26] R.K. Thauer, D. Moller-Zinkhan, and M. Spormann, "Biochemistry of acetate catabolism in anaerobic chemotrophic bacteria," *Annu. Rev. Microbiol.,* pp. 43–67, 1989.

[27] D. Pant, et al., "A review of the substrates used in microbial fuel cells (MFCs) for sustainable energy production," *Bioresource technology*, vol. 101, pp. 1533–1543, 2010.

[28] D.C. Holmes, "Microbe power," *Environmental Health Perspective,* vol. 113, pp. 754-757, 2005.

[29] H. Liu, R. Ramnarayanan, B.E. Logan, "Production of Electricity during Wastewater Treatment Using a Single Chamber Microbial Fuel Cell," *Environmental Science and Technology*, vol. 38, pp. 2281-2285, 2004.

[30]  J.R. Kim, B Min, B.E. Logan, "Evaluation of procedures to acclimate a microbial fuel cell for electricity production," *Applied Microbiology & Biotechnology*, vol. 68, pp. 28-30, 2005.

[31]  B.E. Logan, "Exoelectrogenic bacteria that power microbial fuel cells," *Nature Reviews Microbiology*, Vol. 7, pp. 375-381, 2009.

[32]  B.E. Logan, *Microbial Fuel Cells*, John Wiley & Sons: Hoboken, NJ, 2008.

[33]  H. Ren, et. al., "A high power density miniaturized microbial fuel cell having carbon nanotube anodes," *Journal of Power Sources*, vol. 273, pp. 823-830, 2015.

[34]  B.E. Logan, et al., "Microbial Fuel Cells: Methodology and Technology," *Environmental Science & Technology*, vol. 40, pp. 5181-5192, 2006.

[35]  M. Schechter, et. al, "Anode Biofilm," in *Technology and Application of Microbial Fuel Cells*, InTech, 2014, Ch. 4, Sec. 2, pp. 57.

[36]  Nevin, K.P., et al, "Power output and columbic efficiencies from biofilms of *Geobacter sulfurreducens* comparable to mixed community microbial fuel cells," *Environmental Microbiology*, vol. 10, pp. 2505-2514, 2008.

[37]  B. Gottenbos, H.C. van der Mei, H.J. Busscher, "Models for studying initial adhesion and surface growth in biofilm formation on surfaces," *Methods in Enzymology*, vol. 310, pp. 523-534, 1999.

[38]  M.C.M. van Loosdrecht, et al., "Mathematical modelling of biofilm structures," *Antonie van Leeuwenhoek*, vol. 81, pp. 245–256, 2002.

[39]  T.R. Garrett, M. Bhakoo, Z. Zhang, "Bacterial adhesion and biofilms on surfaces," *Progress in Natural Science*, vol. 18, pp. 1049-1056, 2008.

[40] S.K. Chaudhuri, D.R. Lovley, "Electricity generation by direct oxidation of glucose in mediatorless microbial fuel cells," *Nature Biotechnology*, vol. 21, pp. 1229-1232, 2003.

[41] H.T. Pham, et. Al., "High shear enrichment improves the performance of the anodophilic microbial consortium in a microbial fuel cell", *Microbial Biotechnology*, vol. 1.6, pp. 487-496, 2008.

[42] M. Garren, F. Azam, "New Method for Counting Bacteria Associated with Coral Mucus," *Applied and Environmental Microbiology*, vol. 76, pp. 6128-6133, 2010.

[43] J. Schmidt and E. Zsedely, "Nutrition of Ruminants", Univ. of W-Hungary, 2011, Ch. 1.

[44] J.W. Fatherree. *An Introduction to Tunicates* [Online]. Available: https://www.reefs.com/blog/magazine-parent/2013-2/an-introduction-to-tunicates/

[45] T. Caceci. *Rumen Papillae* [Online]. Available: http://www.doctorc.net/Labs/Lab21/Examples/exrumen.htm

[46] B.E. Logan and J.M. Regan, "Microbial fuel cells: challenges and applications," *Environ. Sci. Technol*. Vol. 40, pp. 5172–5180, 2006.

[47] F. Du, et al., "Continuous flowing membraneless microbial fuel cells with separated electrode chambers," *Bioresource technology*, vol. 102, pp. 8914–8920, 2011.

[48] A. Dewan, H. Beyenal, and Z. Lewandowski, "Scaling up microbial fuel cells," *Environmental science & technology*, vol. 42, pp. 7643–7648, 2008.

[49] J.J. Kane, et al, "An oxygen transfer model for high purity graphite oxidation," *Carbon*, vol. 59, pp. 49–64, 2013.

[50] L.R. Radovic, A.B. Silva-Tapia, and F. Vallejos-Burgos, "Oxygen migration on the graphene surface, origin of epoxide groups," *Carbon*, vol/ 49, pp. 4218–25, 2011.

[51]  B. Erable, et al., "Nitric acid activation of graphite granules to increase the performance of the non-catalyzed oxygen reduction reaction (ORR) for MFC applications," *Electrochemistry communications*, vol. 11, pp. 1547–1549, 2009.

[52]  Y. Wang, "Using Red Blood Cells in Microbial Fuel Cell Catholyte Solution to improve Electricity Generation," M.S. Thesis, Dept. Food, Ag., Bio. Eng., Ohio St. Univ, Columbus, OH, 2014.

[53]  G. Chen, et. al., "Application of biocathode in microbual fuel cells: cell performance and microbial community," *Biotechnnological products and process engineering,* ver. 79, pp. 379-388, 2008.

## Appendix A: Parts, Materials, and Equipment List [25]

**Chemicals**

- Ammonium Chloride (09725-25G), Sigma-Aldrich

- 500 mL 3% Sodium Sulfide (757016), Fisher Scientific

- Sodium acetate (W302406), Sigma-Aldrich

- Dipotassium phosphate (59937), Sigma-Aldrich

- Sodium chloride (S7653), Sigma-Aldrich

- Magnesium sulfate (M7506), Sigma-Aldrich

**Physical Fuel Cell Components**

- Optically Clear Cast Acrylic Sheet 1/4" Thick, 6" x 6" McMaster-Carr #8560k358

- Nafion 117 $10.0 \times 10.0$ cm Fuel Cells Etc.

- Nylon 6/6 Hex Nut Off-White, 10- 32 Thread Size, 3/8" Width, 9/64" Height McMaster-Carr #94812a415

- Optically Clear Cast Acrylic Sheet 1" Thick, $6" \times 6"$ McMaster-Carr #8560k329

- 10-32 x 2 Binder Head Slotted Machine Screws Nylon Fastener-Express

- Watts® SVGEΩ¼-inch (8 mm) OD, 0.170-inch (5 mm) ID, Part #: HSVEB20 clear vinyl tubing

- McMaster-Carr® Nylon 6/6 hex nut, 10-32 thread size (Part #: 94812A415)

- Platinum wire, 0.404 mm, annealed, 99.9% $\approx$ 2.7 g/m (CAS: 7440-06-4, EINECS: 231-116-1), Alfa Aesar

- FDA Luer Lock Polycarbonate Stop Cock (7033T11), McMaster-Carr

- Double/Bubble® Orange High Peel Strength Epoxy Adhesive (04007)

- Silver-based conductive epoxy, Chemtronics® (CW2400)

- Type 316 Stainless Steel Barbed Hose Fitting, Adapter for 1/8" Hose ID × 1/8" NPT

  Male Pipe, MaMaster-Carr (Part #: 535065K61)

**Operational Equipment and Materials**

- 32 oz. Spray bottle with attachment (41101 and 41102), OSU Stores

- Keithley 2100 Digital Multimeter

- 1 L Solvent reservoir with cap (9301-1421), Agilient Technologies

- Cole-Parmer, Low-flow Peristaltic Pump (SP100V1.016CP)

**Computer Software**

- Keithley KI-Link Excel Add-In version 2.03; Keithley Instruments, Inc.

**Overview:**

This document is the protocol for the Microbial Fuel Cell Project in MNSL in Scott W491.

**Project members:**

| | | |
|---|---|---|
| Matt Gerber (Lead) | gerber.117@osu.edu | 614-447-8504 |
| Clare Cui | cui.163@osu.edu | 513-375-9407 |
| Dr. Shaurya Prakash | prakash.31@osu.edu | 217-390-5683 |

**General Guidelines:**

**Personal Protection Equipment (PPE)**

To be worn at all times during experiment operation:
1. Lab coat
2. Goggles
3. Gloves

**Standard Microbiological Practices**
1. Access to the lab is restricted at Dr. Prakash's discretion when work with bacteria cultures is in progress
2. No eating, drinking, smoking, handling contact lenses, applying cosmetics, or storing of food inside the lab
3. Mouth pipetting prohibited
4. Throughout this document, the key term "DEDICATED" refers to: (1) a storage container, (2) a physical workspace, or (3) a piece of equipment that is solely for use in this experiment. That is, no other materials may be stored in DEDICATED storage containers, no other work/experiments may occur within DEDICATED workspaces, and no piece of DEDICATED equipment may be used for purposes other than those specifically outlined in this document.
5. If a storage container, workspace, or piece of equipment listed in this document is not labeled as DEDICATED, then it is assumed to be a shared, laboratory storage container, workspace, or piece of equipment and should follow all safety and cleaning procedures associated with it.
6. DEDICATED storage and work spaces must clearly be labelled at all times with special, bright, ORANGE TAPE.
7. ORANGE TAPE is for the sole purpose of this experiment and should not be used for other reasons
8. Within this document, EXPERIMENT INFORMATION refers to the following, where applicable:
   - The text "MFC Experiment"
   - Contents
   - Creation date
   - Expiration date
   - Experimenter name(s)

9. Work surfaces decontaminated after any spill
10. When running, MFC and associated tubing must be contained within incubator
11. All bacteria not in use is stored in DEDICATED sealed storage container located within shared, laboratory refrigerator

## I. Storage

**Equipment**
1. Refrigerator
2. DEDICATED sealed storage container
3. Celsius thermometer
4. DEDICATED sealed vials/containers marked with ORANGE TAPE

**Procedure**
1. Refrigerator to remain at 4°C at all times
2. Each vial/container labeled with experiment information and ORANGE TAPE
3. Thermometer will remain in refrigerator and will be checked weekly to ensure consistent temperature is maintained
4. Vials/containers to remain inside DEDICATED storage container within refrigerator and are to remain sealed and labeled with experiment information unless in use

## II. PEM Preparation

**Equipment**
1. DI water
2. Tweezers
3. Hot plate
4. Two 200 mL beakers

**Procedure**
1. Disinfect tweezers with 10% bleach solution
2. Pour 150 mL DI water into 200 mL beaker
3. Place beaker on hot plate and bring to a gentle boil at 110°C
4. Place PEM in beaker using tweezers and allow to boil for 1 hour
5. Add DI water as needed to maintain consistent volume
6. After 1 hour, turn off hot plate and allow to cool
7. Fill second 200 mL beaker with DI water and transfer PEM with tweezers to the second beaker
8. If using PEM immediately, transfer to MFC while assembling
9. If PEM is to be stored for future use, cover beaker with parafilm and store on storage rack; label with contents and date prepared

## III. Preparation of Chemicals

**Procedure 1: Creation of 0.4 M NaOH Solution**

1. Crush ~40 pellets (~5 g) of NaOH in mortar and pestle

2. Add 4 g NaOH powder to 250 mL glass storage jar (brown)
3. Add 250 mL DI water and stir with stirring rod until completely dissolved—this is 0.4 M NaOH
4. Seal jar, label with contents and creation date; store along with other bases
5. Shelf life is approximately 1 year


## Procedure 2: Creation of 50 mL Reducing Agent (RA)
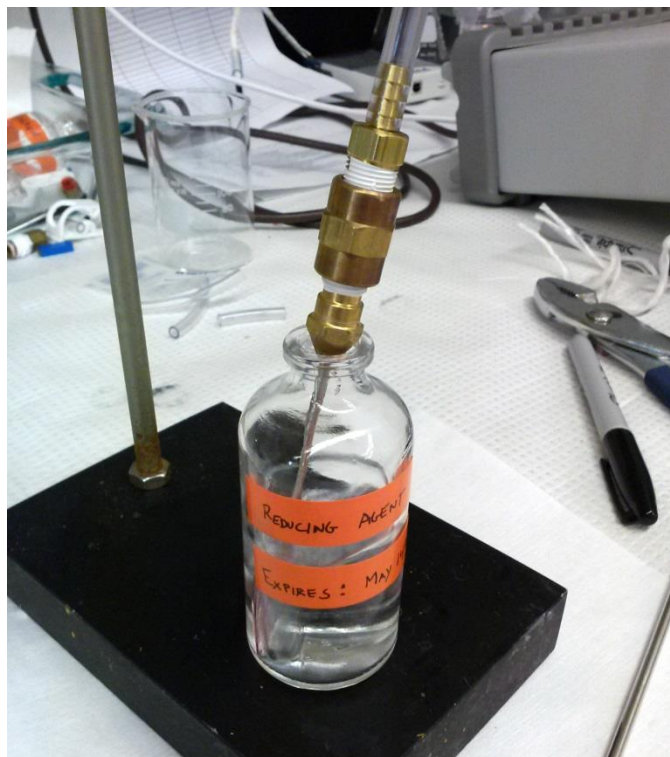*Steps 2–6 must be performed within the fume hood!*



**Figure 1**: Creation of the reducing agent.

1. Add 25 mL of 0.4 M NaOH to small storage vial with rubber stopper
2. *Inside the fume hood, use chemistry ring stand to secure $N_2$ gas line into the vial and begin aerating the NaOH*
3. *Add 1.35 g Cysteine-HCl to the vial, ensuring all solid grains are mixed into the liquid; Aerate with $N_2$ gas for 5 minutes (set a timer)*
4. *To the vial, add 20 mL of 3% w/v $Na_2S$ while continuing to aerate with $N_2$ gas*
5. *To the vial, add 5 mL of DI water while continuing to aerate with $N_2$ gas*
6. *Continue to aerate an additional 10 minutes with $N_2$ (set a timer)*
7. Seal and store at room temperature; Indicate contents and expiration date on bottle
8. Reasonable shelf-life is 1 week and should be used within this time frame

## Procedure 3: Creation of 1 L of Substrate Feed

1. Clean container for storing substrate (hereafter called "reservoir"); See Part V

2. Fill reservoir with 1 L of DI water
3. Add parafilm to reservoir top (to protect the contents from particles in the air)
4. Ensure 50 mL of reducing agent has been created; keep it accessible nearby
5. Place reservoir on magnetic stirrer, add stir bar, set to 400 rpm; Ensure a nice "tornado" spiral forms in the center of the reservoir
6. Weight and add 5 g of Sodium acetate and start a timer (Sodium acetate requires 10 minutes to dissolve)
7. Next, weigh and add the following compounds in the order below to the reservoir:

| Component | Formula | Amount |
|---|---|---|
| Dipotassium phosphate | $K_2HPO_4$ | 0.9 g |
| Ammonium chloride | $NH_4Cl$ | 0.73 g |
| Sodium chloride | $NaCl$ | 0.9 g |
| Magnesium sulfate | $MgSO_4$ | 0.09 g |

8. These components should dissolve immediately; Allow timer to reach at least 10 minutes then check if any undissolved particles remain. If so, allow to stir until no particles remain.
9. Reapply parafilm to reservoir top and transfer to chemistry ring stand inside the fume hood
10. Insert $N_2$ gas tube into reservoir and bubble gas through for 10 minutes, turning the reservoir 180° every minute or so
11. While the $N_2$ is bubbling through the reservoir, towards the end of the 10 min, add the 50 mL of reducing agent. Do this slowly and ensure no air bubbles are being mixed in.
12. Calibrate pH meter and insert probe into substrate feed. Add 0.1 M HCl until pH is 6.8.
13. At this point, there is 1 L of substrate feed in the reservoir and it is ready to be used in the continuous flow setup.
14. For 1 L of substrate feed in a storage jar, simply repeat the above procedures using a 1 L storage jar
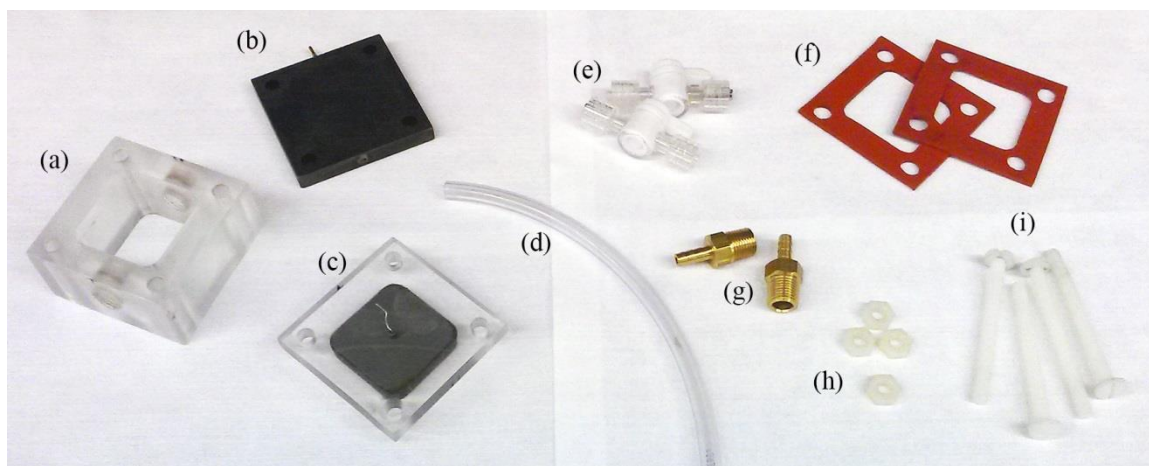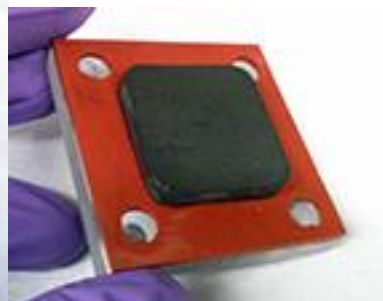15. Use HCl and NaOH to change the pH to 6.8

## IV. Assembling MFC

**Figure 2:** All components for MFC: (a) main chamber, (b) cathode, (c) anode end cap, (d) tubing, (e) valves, (f) rubber gaskets, (g) brass ports, (h) hex nuts, and (i) bolts.
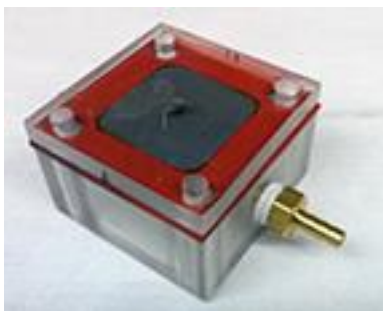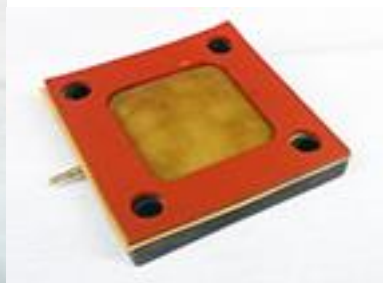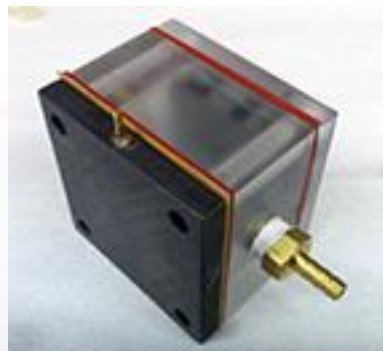


(a)

(b)

(c)

(d)

(e)

(f)

(g)

(h)

**Figure 3:** Assembly process for MFC.

**Equipment**
1. All physical MFC components (Figure 1)
2. Wrench
3. Flathead screwdriver (larger the better)
4. Teflon tape

**Procedure**
1. Gather all physical MFC components. Components are:
    a. Main chamber
    b. Pre-assembled anode component
    c. Graphite cathode
    d. Four nylon 10-32 bolts
    e. Four nylon 10-32 hex nuts
    f. Two (2) silicone rubber gaskets
    g. PEM
2. Add Teflon tape to brass ports (Figure 3a)
3. Screw ports into main chamber (Figure 3b)
4. Fit one rubber gasket over anode (Figure32c)
5. Fit anode with gasket into main chamber, hold together with fingers (Figure 3d)
6. Add PEM and second rubber gasket to cathode, with PEM sandwiched between the cathode and the gasket (Figure 3e)
7. Add result of Step 6 to main chamber (Figure 3f), lining up the holes
8. Fit 4 nylon bolts through each hole; the head of the bolt should be on the cathode side (the nuts should go on the anode side—important!)
9. Secure nuts with fingers and once tight, tighten further with wrench and screwdriver. Result should look like Figure 3g
10. Add about 1 inch of tubing to each port
11. Add valve to each bit of tubing (Figure 3h)
12. At this point, MFC should be fully sealed and open to air only through the ports

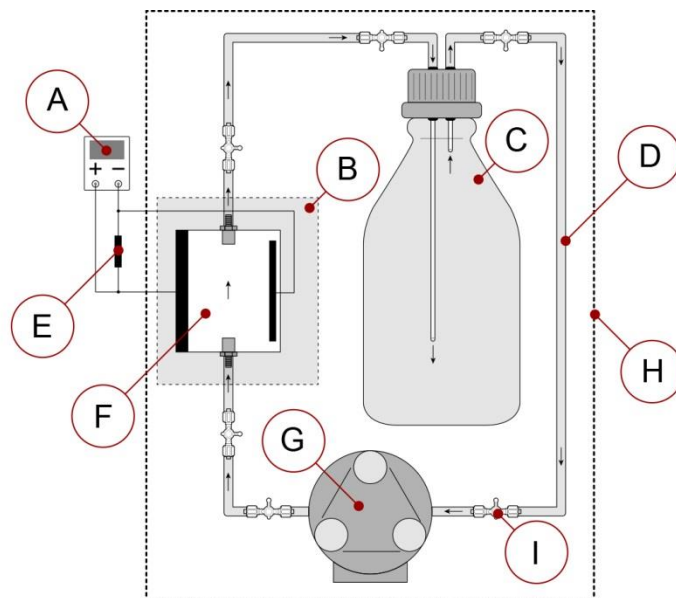**V. Setting Up Continuous Flow Mode**

**Figure 4**: Schematic for continuous flow setup.

**Equipment**
1. Assembled MFC
2. Six luer-lock valves
3. 1 L substrate reservoir (filled)
4. 1 L storage jar of substrate (filled)
5. Various lengths of tubing
6. Peristaltic pump
7. Reservoir cap with attached inner tubing (short and long)
8. Hot plate
9. Insulation box
10. 10 mL disposable syringe

**Procedure**
1. Attach 2-cm length of tubing to brass fittings on MFC
2. Onto both pieces of tubing, attach luer-lock valves
3. Using 10 mL syringe, fill MFC with substrate, ensuring no bubbles remain in the main chamber. To do so, open both valves, fill the syringe with substrate, attach syringe to one valve, then physically hold the MFC so that the other valve is pointed towards the ceiling. Squeeze the syringe, filling the main chamber with 10 mL of substrate. With syringe still attached, close both valves then remove syringe. Fill syringe with substrate, attach to valve, hold the other valve towards the ceiling, open both valves, and continue to fill.
4. Repeat previous step until no bubbles are in the main chamber, then close both valves and place MFC onto hotplate at 50°C.
5. Using tubing, connect outlet valve to Peristaltic pump using an additional luer-lock valve. To do so, secure the empty tubing the syringe, use it to suck up substrate (filling the tubing), then attach the tubing to the luer-lock valve. Ensure the valve is closed, then remove the syringe. A full piece of tubing should be attached to the valve. Connect this to another luer-lock valve and secure this valve to the pump. This process should be used for all other tubing connections in this procedure.

6.  Top off reservoir with substrate from the storage jar and then add reservoir cap to reservoir
7.  Connect Peristaltic pump outlet to a luer-lock valve and tubing to the inlet of the reservoir (if reservoir inlet/outlet not labeled, the inlet is the port connected to the *smaller* inner tube).
8.  Connect reservoir outlet to a luer-lock, which itself is connected to the luer-lock already attached to the inlet of the MFC
9.  Place insulation box on top of hot plate and over MFC
10. With all valves closed and the pump off, the MFC is on batch-fed mode.
11. For continuous-flow operation, open all valves *before* turning on the pump

## VI. Electronics

**Equipment**
1.  MFC in continuous-flow setup, from Part V
2.  1 kΩ resistor
3.  Two alligator-clip leads
4.  DMM with alligator clip banana plug leads
5.  Faraday cage with banana plug grounding lead
6.  Ferrite beads, assorted sizes

**Procedure**
1.  Using alligator clip leads, connect resistor to anode and cathode in series
2.  Connect DMM in parallel to the resistor
3.  Place Faraday cage over entire setup, excluding the DMM, and ground the cage to the DMM
4.  If possible, place ferrite beads on the ends of all leads
5.  Ensure there is an electrical connection between the ground and the Faraday cage

## VII. Cleaning and Emptying

**Part 1: Creating 10% Bleach Solution**

**Equipment**
1.  Bottle of commercially available Clorox bleach
2.  Tap water
3.  Bleach solution bottle.

**Part 1 Procedure**
1.  Fill bleach solution bottle to line indicated "10% fill line" with Clorox blean
2.  Fill bleach solution bottle to line indicated "Fill line" with tap water
3.  Seal bottle and store beneath sink

**Part 2: MFC Disassembly and Cleaning**

**Equipment**
1.  One (1) 1000 mL beaker
2.  10% bleach solution from Procedure 1
3.  DEDICATED liquid contaminated waste container

    4. Paper towels
    5. DEDICATED solid waste container

**Part 2 Procedure**
1. Turn off electronics, unplug, and detach MFC from leads
2. Ensure all valves are closed
3. Disconnect all valves and tubes and place into 1000 mL beaker
4. Remove reservoir cap and dump reservoir into liquid contaminated waste container along with 1 L of 10% bleach solution
5. Remove MFC from hot plate and empty into 1000 mL beaker
6. Dissemble MFC, placing each component into the 1000 mL beaker
7. Fill beaker with 10% bleach solution and allow to soak for 10 minutes
8. Empty contents into contaminated waste container
9. Rinse components with tap water 3–4 times, then clean each with soap, rinse again 3–4 times with tap water
10. Finally, fill beaker with DI water, allow to sit for 5 minutes, then remove components and dry with paper towels
11. For the reservoir, rinse with 10% bleach solution, dump into contaminated waste container
12. Wash inside with soap, ensuring all particles are removed from the inside.
13. Rinse with tap water 3–4 times, rinse with acetone, rinse again with tap water 3–4 times, then finally rinse with DI water before air drying (do NOT dry inside with paper towel)

**Part 3: Comprehensive List of Equipment Cleaning**

**Cleaning Equipment for all Lists**
1. 10% bleach solution from Step 1
2. DEDICATED liquid contaminated waste container
3. DEDICATED solid waste container
4. Paper towels

**List 1: Glass Equipment**
1. DEDICATED beakers, various sizes
2. DEDICATED graduated cylinders, various sizes
3. DEDICATED glass stirring rod
4. DEDICATED 20 mL scintillation vials
5. DEDICATED 10 mL test tubes

**List 1 Cleaning Process**
1. Rinse all surfaces with 10% bleach solution
2. Wash with soap and water
3. Rinse 3–4 times with tap water, then with acetone, then 3–4 with tap water, then finally with DI water
4. Set out paper towels and place cleaned equipment on to dry
5. Once equipment is dry, can be reused or thrown away
6. Dispose of used paper towels in DEDICATED solid waste container

**List 2: Non-glass Equipment**
1. Tweezers
2. DEDICATED rubber stopper for flasks

**List 2 Cleaning Process**
1. To 500 mL beaker, add component
2. Fill beaker with 10% bleach solution, ensuring components/equipment are fully immersed
3. Allow beaker to sit for 10 minutes
4. Empty liquid components of beaker into DEDICATED liquid contaminated waste container
5. Wash component with soap and water, rinse with water 3–4 times, then rinse with DI water
6. Set out paper towels and place cleaned components/equipment on to dry
7. Clean empty beaker according to laboratory procedures for non-contaminated materials
8. Once components/equipment is dry, can be reused or thrown away
9. Dispose of used paper towels in DEDICATED solid waste container

**List 3: Storage and Work Spaces**
1. Laboratory refrigerator
2. Sealed, storage container
3. Tabletop workspace
4. Workspace within fume hood
5. Incubator

**List 3 Cleaning Process**
1. Wipe down surface with paper towels
2. Dispose of paper towels in DEDICATED solid waste container
3. Soak DEDICATED sponge with 10% bleach solution
4. Scrub surface with sponge
5. Dispose of sponge in DEDICATED solid waste container
6. Dry surface with paper towels
7. Dispose of paper towels in DEDICATED solid waste container

**V. Disposal**

**Disposal Resources**
1. Sharps container
2. DEDICATED liquid contaminated waste container
3. DEDICATED solid waste container

*When a piece of equipment breaks, is no longer required, or has otherwise been rendered unusable, follow these disposal procedures. Disposal procedures are unique to each piece of equipment used.*

**Solid materials:**
1. MFC Main chamber
   a. Wipe down with sponge and bleach solution
   b. Place in solid waste container
2. MFC Anode component
   a. Decontaminate in a 250 mL beaker with 200 mL bleach solution for 10 minutes
   b. Place in solid waste container
3. MFC Cathode end plate
   a. Decontaminate in a 250 mL beaker with 200 mL bleach solution for 10 minutes

       b.   Place in solid waste container

4.  MFC Cathode graphite
       a.   Decontaminate in a 250 mL beaker with 200 mL bleach solution for 10 minutes
       b.   Place in solid waste container

5.  MFC Bolts, Washers, and Nuts
       a.   Decontaminate in a 250 mL beaker with 200 mL bleach solution for 10 minutes
       b.   Place in solid waste container

6.  MFC 1/8 in. tubing
       a.   Decontaminate in a 250 mL beaker with 200 mL bleach solution for 10 minutes
       b.   Place in solid waste container

7.  MFC 1/8 in. valves
       a.   Decontaminate in a 250 mL beaker with 200 mL bleach solution for 10 minutes
       b.   Place in solid waste container

8.  MFC rubber gaskets
       a.   Decontaminate in a 250 mL beaker with 200 mL bleach solution for 10 minutes
       b.   Place in solid waste container

9.  $150 \times 15$ mm plastic Petri dishes
       a.   Decontaminate in a 250 mL beaker with 200 mL bleach solution for 10 minutes
       b.   Place in solid waste container

10. Paper towels
       a.   Place in solid waste container

11. Sponges
       a.   Decontaminate in a 250 mL beaker with 200 mL bleach solution for 10 minutes
       b.   Place in solid waste container

12. Disposable pipettes
       a.   Decontaminate in a 250 mL beaker with 200 mL bleach solution for 10 minutes
       b.   Place in solid waste container

13. Glass scintillation vials
       a.   Decontaminate in a 250 mL beaker with 200 mL bleach solution for 10 minutes
       b.   Place in solid waste container

14. Cleaning tray
       a.   Decontaminate in a 250 mL beaker with 200 mL bleach solution for 10 minutes
       b.   Place in solid waste container

15. Syringes and needles
       a.   Place in sharps container; do not recap

16. Incubator
       a.   Dispose in solid waste container large outdoor trash receptacle

17. Glass beakers
       a.   Place in solid waste container

18. Glass Erlenmeyer flasks
       a.   Place in solid waste container

19. Pump
       a.   Attach tubing to outlet and inlet of pump
       b.   Fill a 250 mL beaker with 200 mL bleach solution and place inlet tubing in solution
       c.   Take an empty 250 mL beaker and place outlet tubing inside
       d.   Allow pump to run until all bleach solution has reached the empty beaker

20. Glove bag
       a.   Compress bag
       b.   Dispose in solid waste container

21. Rubber stoppers
    a. Decontaminate in a 250 mL beaker with 200 mL bleach solution for 10 minutes
    b. Place in solid waste container
22. Thermometers
    a. Place in solid waste container
    b. If broken, dispose of in sharps container

**Liquid materials:**
1. Substrate feed solution
    a. Can be poured down the sink drain with faucet on
2. Bacteria solution
    a. Mix in bleach solution at a 1:1 ratio
    b. Pour liquid into liquid contaminated waste container

**General Procedure**
1. All surfaces, containers, and components exposed to cultures must be decontaminated with bleach solution prior to disposal
2. Bleach solution must remain in contact with materials for 10 minutes when decontaminating
3. Do not re-cap, bend, break, or remove needles prior to disposal; needles must be disposed of in laboratory sharps container
4. Dispose of bleach solution by rinsing with water into sink drain

## VI. Accidents/Spills

**Equipment**
1. Paper towels
2. 10% bleach solution
3. DEDICATED sponges

**List of Contingency Plans**
1. If refrigerator breaks and 4°C is not maintained (bacteria may be unusable) and vials must be thrown out
    a. Empty vials into liquid contaminated waste container
    b. Dispose of vials in solid waste container
2. Mysterious storage vial appears (someone forgot to label it); the contents cannot be confirmed/known
    a. Empty vial into liquid contaminated waste container
    b. Dispose of vial in solid waste container
3. DEDICATED sealed storage container within laboratory refrigerator breaks (is no longer air-tight or sealed)
    a. Check to see if any scintillation vials have broken
    b. If no, replace storage container with another that can be sealed and dispose of old in solid waste container
    c. If yes, empty refrigerator shelf that container was stored on, including any other chemicals
    d. Wipe down shelf and other items with paper towel soaked in bleach solution
    e. Wipe down glass scintillation vials with bleach solution
    f. Replace broken storage container with working sealed container and place vials back inside

4. Someone forgot to reseal the storage container within laboratory refrigerator
    a. Remove storage container and check refrigerator for any spills
    b. If spillage occurred, remove contents and wipe down area with bleach solution and paper towels
    c. Wipe down contents with bleach solution and paper towels, including storage container
    d. Seal storage container
    e. Replace everything back into refrigerator
5. Sodium acetate contaminates laboratory analytical scale
    a. Dust off sodium acetate into a paper towel and dispose of in solid waste container
    b. Wipe with paper towel soaked in bleach solution
    c. Dispose of all paper towels in solid waste container
6. Sodium acetate falls onto laboratory floor
    a. Wipe up sodium acetate with a wet paper towel soaked in water
    b. Wipe area with paper towel soaked in bleach solution
    c. Dispose of all paper towels in solid waste container
7. Substrate feed escapes workspace spilltray and contaminates desktop surface or floor
    a. Wipe up substrate feed with a wet paper towel soaked in water
    b. Wipe area with paper towel soaked in bleach solution
    c. Dispose of all paper towels in solid waste container
8. HCl escapes workspace spilltray and contaminates desktop surface or floor
    a. Spread a neutralizing powder onto contaminated area
    b. Collect powder and dispose of in solid waste container
    c. Wipe over area with paper towels soaked in bleach solution
    d. Dispose of paper towels in solid waste container
9. NaOH escapes workspace spilltray and contaminates desktop surface or floor
    a. Spread sand, earth, or a similar material onto contaminated area
    b. Collect material and dispose of in solid waste container
    c. Wipe over area with paper towels soaked in bleach solution
    d. Dispose of paper towels in solid waste container
10. Beaker/flask containing bacteria and broth falls to floor and breaks
    a. Use a dustpan and paper towels to sweep broken pieces and soak up broth
    b. Throw paper towels into solid waste container
11. Needle punctures someone's skin
    a. Throw away needle into sharps container
    b. Clean skin with alcohol pads from first aid kit
    c. Bandage affected area
12. Flask leaks inside incubator
    a. Turn off incubator
    b. Remove flask from incubator
    c. Pour liquid inside flask into another flask with no cracks
    d. Wipe inside of incubator with paper towels and bleach solution
    e. Place flask back inside and turn on incubator once more
13. Syringe filled with bacteria solution punctures someone's skin
    a. Contact others for help immediately
    b. Empty syringe contents into liquid contaminated waste container
    c. Throw away needle and barrel into sharps container
    d. Clean skin with alcohol pads from first aid kit
    e. Bandage affected area
14. Scintillation vial falls to floor and breaks

a. Use a dustpan and paper towels to sweep broken pieces and soak up broth
    b. Throw paper towels into solid waste container
15. MFC is not fully sealed and air-tight and begins to leak during construction phase
    a. Finish construction completely; MFC is expected to leak a small amount during construction
    b. After construction, take out MFC and wipe down with dry paper towel
    c. Pour excess fluid from catch tray into liquid contaminated waste container
    d. Wash catch tray with sponge and bleach solution
16. MFC leaks into Petri dish, or otherwise cannot retain fluid and leaks inside incubator
    a. Deconstruct MFC inside catch tray
    b. Wash MFC and reconstruct as in Part III
    c. Pour fluid in catch tray into liquid contaminated waste container
    d. Wash and dry catch tray with bleach solution and paper towels
17. We drop the fully sealed MFC onto the floor and it breaks open, damaging some parts
    a. Deconstruct MFC inside a catch tray and determine which parts are broken
    b. Dispose of broken parts into solid waste container
    c. Clean up any liquid on floor with paper towels
    d. Sanitize with bleach solution and then wipe dry with paper towels
    e. Dispose of paper towels into solid waste container
18. Bottle of concentrated bleach spills onto floor or into workspace
    a. Remove all equipment from area to a dry location
    b. Wipe up spill with paper towels
    c. Soak paper towels in water and wipe over spill area twice

**General Clean-Up Guidelines**
*The above list is not assumed to be comprehensive. The following is a list of clean-up guidelines for general accidents and spills.*
1. Remove all associated equipment from contaminated area and place in sink
2. If equipment is broken and needs to be disposed, refer to Part V for proper disposal method
3. Wipe down equipment with paper towels soaked in bleach solution
4. Soak up spill with paper towels
5. Clean contaminated surface with bleach solution
6. Leave bleach in contact with surface for 10 minutes
7. Wipe up bleach with paper towels
8. Paper towels disposed of in contaminated waste container
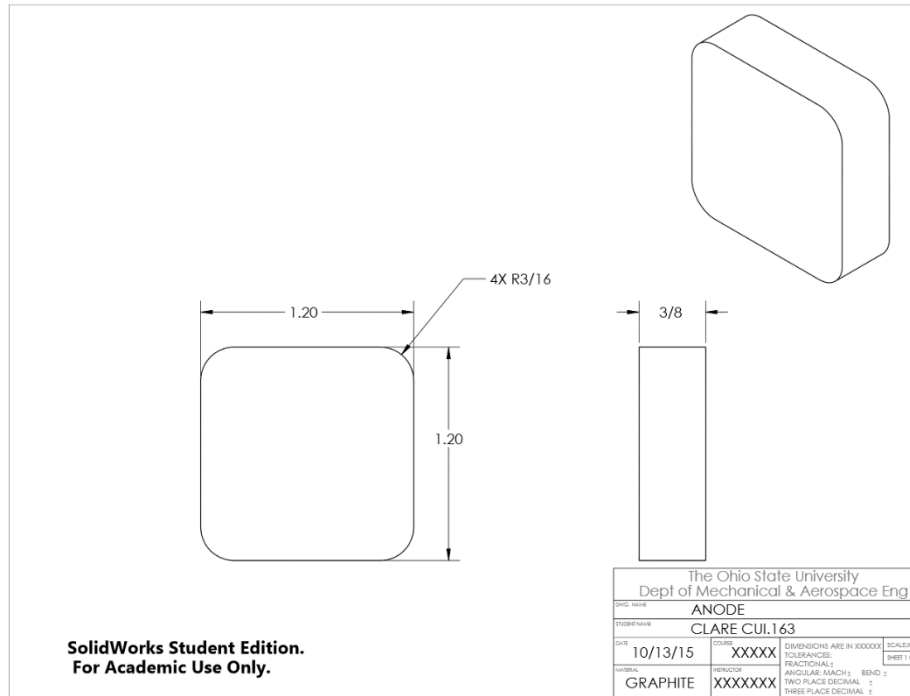
**Appendix C: Engineering Drawings for MFC**



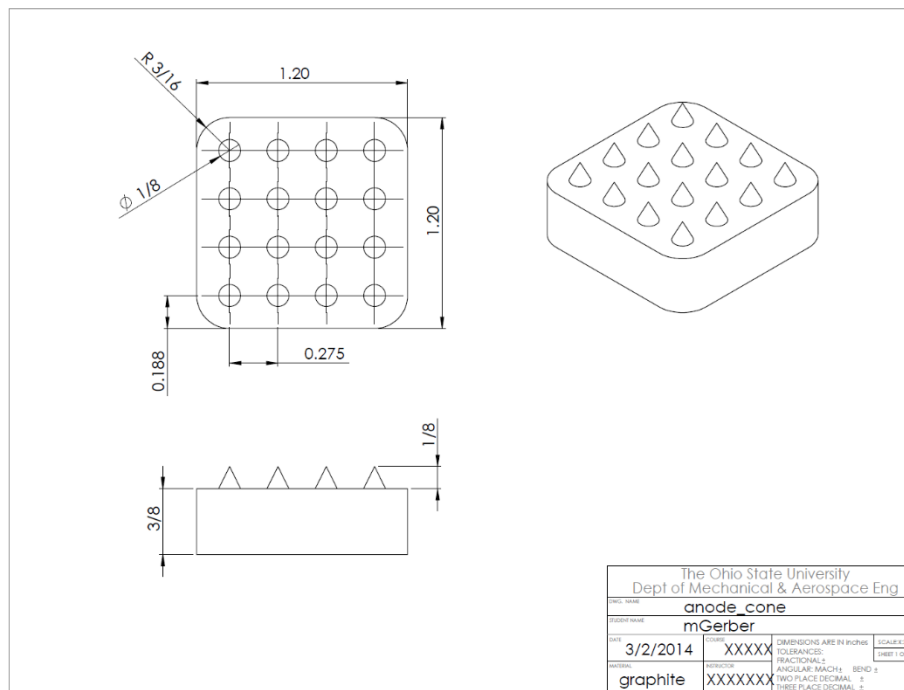*Figure C 1: Engineering drawing for flat anode.*



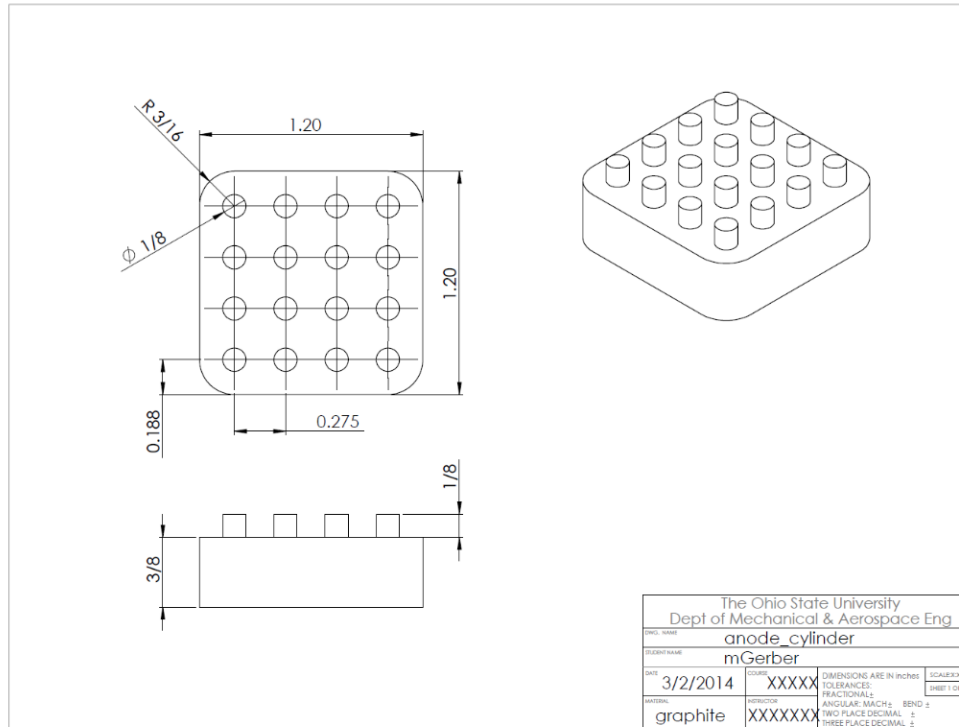*Figure C 2: Engineering drawing for patterned cones design.*

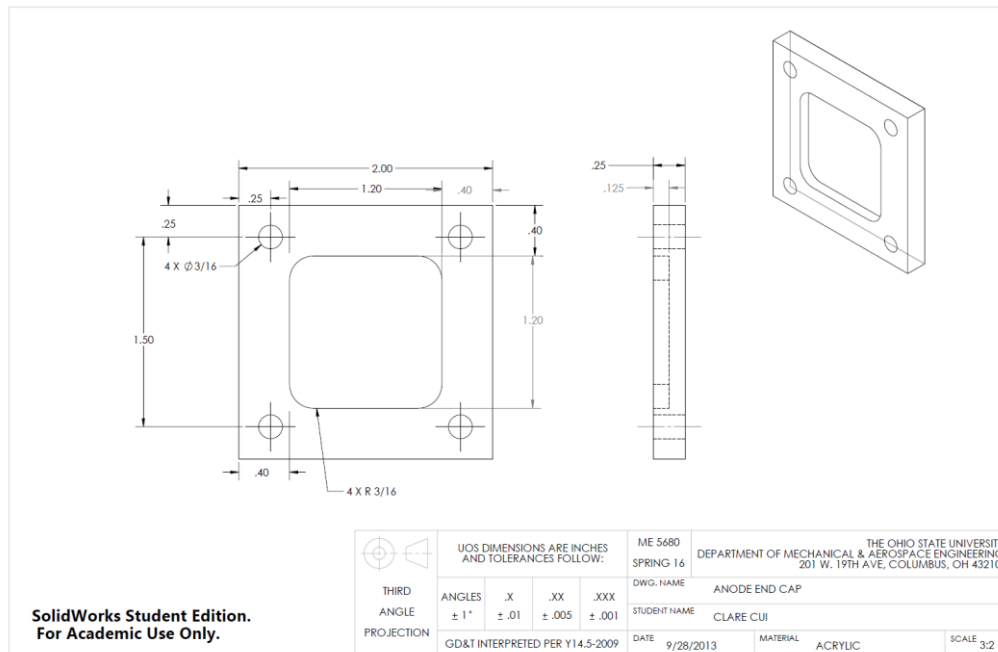*Figure C 3: Engineering drawing for patterned cylinders design.*

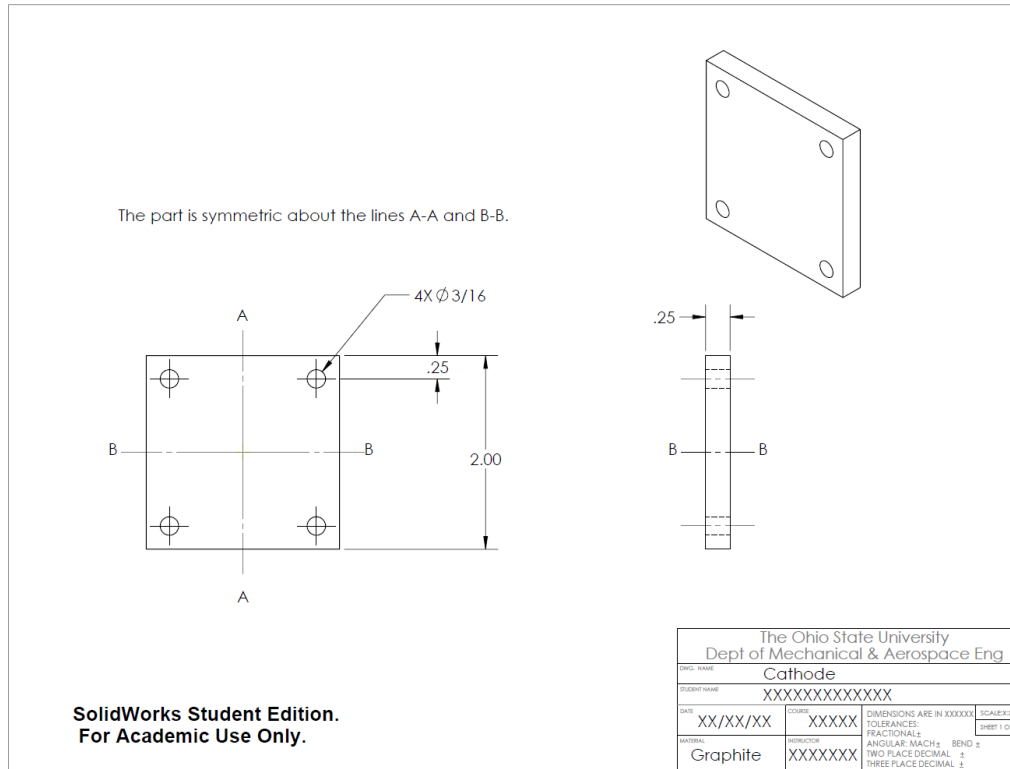

*Figure C 4: Engineering drawing for anode end plate*
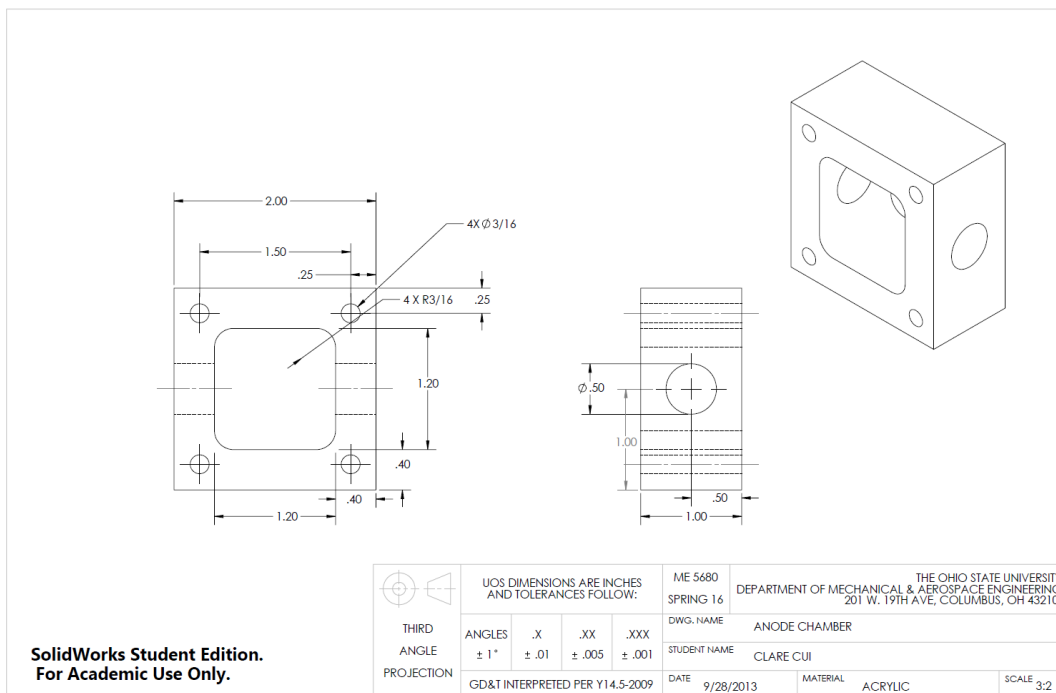
C2

***Figure C 5:*** *Engineering drawing for graphite cathode.*



***Figure C 6:*** *Engineering drawing for anode chamber.*